Decentralized Formation and Attitude Control of Spacecraft

Submitted in partial fulfillment of the requirements
of the degree of

Bachelor of Technology

by

Aaron John Sabu
(Roll No. 170070050)

Supervisor:
Prof. Dwaipayan Mukherjee

Department of Electrical Engineering
INDIAN INSTITUTE OF TECHNOLOGY BOMBAY
Fall 2020

Dedicated to God Almighty for everything in my life,

particularly my beloved parents and sister,

my institution, advisor, and instructors,

and my friends and supporters.

Declaration

I declare that this written submission represents my ideas in my own words and where others ideas or words have been included, I have adequately cited and referenced the original sources. I also declare that I have adhered to all principles of academic honesty and integrity and have not misrepresented or fabricated or falsified any idea/data/fact/source in my submission. I understand that any violation of the above will be cause for disciplinary action by the Institute and can also evoke penal action from the sources which have thus not been properly cited or from whom proper permission has not been taken when needed.

Aaron John Sabu

Date:

Roll No. 170070050

Acknowledgments

I wish to record a deep sense of gratitude to my supervisor, **Prof. Dwaipayan Mukherjee** for his valuable guidance and constant support throughout the B.Tech project. He was always available at a very short time's notice, accepted my ignorance in topics with an open heart, and was totally willing to spend time for advising and providing feedback about the work.

I am extremely grateful to my father, **Sabu John**, my mother, **Jessy Sabu John**, and my sister, **Priscilla Thankam Sabu**, for supporting me and providing a serene environment throughout the progress of the project. I strongly believe that achieving goals would have been a matter of great worry in these challenging times if not for their cooperation and backing.

Finally, I am thankful to everyone who has made a positive impact on my life and undergraduate career, including instructors who have personally guided me throughout my studies, and all my friends and peers who have always been a support.

Abstract

The social nature of humankind demands communication and transportation at extremely high rates. Over the 20th and 21st centuries, we have witnessed several advancements in these fields, not only regarding the front-end devices, but also with respect to the satellites that facilitate fast communication and localization. These satellites require to form formations at precise locations with accurate attitudes and velocities. However, controlling them from a ground station on earth does not provide the required amounts of accuracy due to the non-zero communication lags and possibilities for the lack of communication channels.

This calls for the necessity of a decentralized formation algorithm between the satellites to coordinate themselves for human activities. It is also required that the satellites are capable of aligning themselves based on the collective decisions made by the group. As a result, each satellite requires an attitude control mechanism to control their heading and angular velocities. This should be blended with the formation control algorithm.

This report deals with studies that have been on these two topics individually and collectively. Attitude control and maneuver strategies have also been collected from a renowned textbook in the field. Following this, the results obtained in the studies are explained along with possible scopes of improvement. Finally, the report provides a picture of how research on this field can move forward in the future with the ideas obtained from the above sources.

Contents

List of Figures

List of Abbreviations

ACS	Attitude Control System
AOCS	Attitude and Orbit Control System
cm	center of mass
CPGA	Continuous Path Generation Algorithm
ES	Earth Sensor
GEO	GEostationary Orbit
GNC	Guidance, Navigation, and Control
GTO	Geosynchronous Transfer Orbit
IMU	inertial Measuring Unit
LP	Low Pass
MAS	Multi-Agent Systems
MW	Momentum Wheel
RIG	Rate Integrating Gyroscope
RWA	Reaction Wheel Assembly
s/c	spacecraft
SDE	Stochastic Differential Equation

Chapter 1

Introduction

1.1 Background

It is an everyday phenomenon to see how ants run about searching for food and other resources. Usually, anything on the ground is picked up within a few minutes and transported to an ant colony several meters away. And this task is usually not carried out by a single individual but by tens if not hundreds and thousands of ants, hence making the entire process faster and more efficient. It is quite impossible to imagine a queen ant or another form of centralized center dictating commands to each ant on the location, quality and size of the food source. Yet, as shown in Figure 1.1, they manage to bring their dinner home following an on-site party. This is an ideal example for decentralized control.

The motivation from ants can be extrapolated into human activities. Man has always required a reliable source of communication, and in the latest times, has come up with satellite constellations such as the famous Iridium constellation and SpaceX's upcoming Starlink constellation to manage communication across the planet. Future missions involving multiple spaceships traveling to extraterrestrial bodies will similarly utilize similar forms of control for proper communication and to remain in the proper trajectory. However, individual satellites and spaceships will also require mechanisms of their own to maneuver themselves, hence necessitating the need for proper attitude control techniques which need to be integrated with decentralized formation algorithms for achieving the desired goals.

Figure 1.1: Ants transporting sugar crystals

1.2 Motivation

- Decentralized formations, when compared to centralized equivalents or to conglomerated modules, can perform tasks at higher rates and with higher efficiency, while usually utilizing smaller energy levels.
- Decentralized formation control is an active area of research in control theory due to the constant need for better algorithms and techniques to achieve desired trajectories with the least number of constraints.
- Despite the practical scope of the field, there is very little research on the physical implementation of novel algorithms while incorporating spacecraft dynamics.

1.3 Research objectives

This thesis presents a conglomeration of ideas in the fields of spacecraft attitude control along with decentralized formation control. The information described in the thesis is based on a literature survey of several publications in these fields as well as the reading of relevant portions from a textbook on spacecraft dynamics and control. Furthermore, possible aspects of development are also presented based on the work performed in these resources.

1.4 Thesis outline

The subject matter of the thesis is presented in the following five chapters,

- ✓ Chapter 2 gives an overview of relevant topics on spacecraft attitude control as learned from 'Spacecraft Dynamics and Control' by Marcel J Sidi. Ideas specific to the project are described in detail along with relevant peripheral information.
- ✓ Chapter 3 elucidates the basic principles used in relevant literature on multi-agent formation control along with the corresponding algorithms and schemes, and Chapter 4 gives detailed explanations on previous research in this field that had been developed with the objective of spacecraft formation flying and similar outer-space-based operations.
- ✓ Chapter 5 describes recent developments in the field of attitude control, hence linking to the traditional approaches adopted in earlier research that has been incorporated in the textbook (described in Chapter 1).
- ✓ Chapter 6 discusses in detail the simulation results obtained from algorithms as explained in the corresponding papers from chapters 4 and 5.
- ✓ Chapter 7 provides concluding remarks on the research works that are discussed throughout the report, along with the pros and cons of the techniques used in them.
- ✓ Chapter 8 gives an explanation of my learnings from the project and the directions in which it can further be progressed. Also discussed are the possible aspects in which the schemes discussed in the publications may be improved to provide superior results.

Chapter 2

Traditional Concepts on Spacecraft Attitude Control

2.1 Introduction

This chapter is based on the reading of the textbook on 'Spacecraft Dynamics and Control: A Practical Engineering Approach' by Sidi (1997). Relevant information has been described in detail and supporting concepts have been explained as well.

2.2 The Spacecraft in Consideration

The theories, computations and statements made in the book revolve around the design of a geostationary satellite, although parameters vary with context. The first chapter begins by describing a geosynchronous communications satellite that minimally consists of a central body, solar arrays, an antenna tower, and controller and attitude sensors. The AOCS hardware of the satellite may include a reaction bipropellant thrust system, momentum wheels, horizon sensors, sun sensors, gyros, etc. The mission sequence consists of launch into geosynchronous transfer orbit (GTO), transfer to geostationary orbit (GEO), calibration of the AOCS, and finally the preparation of the satellite for the actual GEO mission. The apogee boost motor (ABM) is used for transfer of orbits.

2.3 Orbit Dynamics

2.3.1 A Revision of Physical Definitions, Laws and Theorems

Newton provided three laws of mechanics and one for gravitation attraction. Kepler further stated three empirical laws: the orbit of a planet is an ellipse with the sun at one focus; the radius vector drawn from the sun to a planet sweeps equal areas in equal time intervals (the law of areas); and, the cube of the planetary period of revolution is proportional to the square of the mean distance of the planet to the sun. The moment of a force $\mathbf{F}$ about the origin O on a particle m with position vector $\mathbf{r}$ is given by $\mathbf{M} = \mathbf{r} \times \mathbf{F}$. The moment is equal to the time rate of change of its moment of momentum or angular momentum $\boldsymbol{h}$, irrespective of whether the mass is variable or the force is non-conservative. Angular momentum remains constant for motion in a force field characterized by an inverse square law. For $\mu = GM$,

$$\frac{d^2r}{dt^2} - r\left(\frac{d\theta}{dt}\right)^2 = -\frac{\mu}{r^2}$$

Using substitutions and further mathematical formulation, we get $\frac{1}{r} = u = \frac{\mu}{h^2} + c\cos(\theta - \theta_0)$, where c is the integration constant calculated from the *total energy per unit mass* $E = \frac{v^2}{2} - \frac{\mu}{r}$. Hence we obtain $E = \frac{h^2c^2}{2} - \frac{\mu^2}{2h^2}$, giving $c = \frac{\mu}{h^2}\sqrt{1 + 2E\frac{h^2}{c^2}}$.
We define *eccentricity* as $e = \sqrt{1 + 2E\frac{h^2}{c^2}}$, giving us: $E = (e^2 - 1)\frac{\mu^2}{2h^2}$. Replacing the substitution $u = \frac{1}{r}$ gives us the final equation for Keplerian orbits ($p = \frac{h^2}{\mu}$ = semi-latus rectum):

$$r = \frac{p}{1 + e\cos(\theta - \theta_0)}$$

For an elliptic orbit, the shortest and longest radius vectors between the prime focus and a point on the ellipse have lengths $r_p = p/(1+e)$ and $r_a = p/(1-e)$ respectively, and the corresponding points are called *periapsis* and *apoapsis* respectively. Eccentricity is related to these lengths as $e = \frac{r_a - r_p}{r_a + r_p}$. Parabolic orbits represent the orbits adopted by a spacecraft while escaping a planet's gravitational field, giving the escape velocity from $v^2 = 2\mu/r$. Hyperbolic orbits are useful for transplanetary spacecraft voyages. For θ and ψ defined as the true anomaly and the eccentric anomaly respectively, we get: $\tan(\theta/2) = \sqrt{\frac{1+e}{1-e}}\tan(\psi/2)$. Hence,

$$r = a(1 - e\cos\psi)$$

2.3.2 Definition of Parameters for Keplerian Orbits in Space

An inertial reference frame can be defined for an earth-orbiting spacecraft as follows: the origin is at the center of mass of the Earth; the **Z** axis is the axis of rotation of the Earth in the positive direction; the **X** axis is the *vernal equinox* vector formed by the intersection of the equatorial plane with the ecliptic plane (plane of Earth's orbit around the Sun) at 22.5°; and the **Y** axis is defined by completing the orthogonal right-handed system. The X axis intersects the celestial sphere at the *vernal point* or *first point of the Aries* (♈).
The classical orbit parameters are given by a vector $\boldsymbol{\alpha}$ with components:

- a: the *semi-major axis* of the ellipse,
- e: the *eccentricity* of the ellipse,
- i: the *inclination*, i.e., the angle made between the orbit and the earth's equatorial plane,
- Ω: the *right ascension* of the ascending node, i.e., the angle in the equatorial plane that separates the node line from the $\boldsymbol{X}_{\Upsilon}$ axis,
- ω: the *argument of perigee*, i.e., the angle between the radius vector of the moving body ($\boldsymbol{r}$) and the the radius vector of the perigee ($\boldsymbol{r_P}$), and
- $M = n(t - t_0)$: the mean anomaly, where n is the mean motion.

where the *node line* is the line of intersection of the orbital plane and the equatorial plane. These parameters are represented in Figure 2.1:

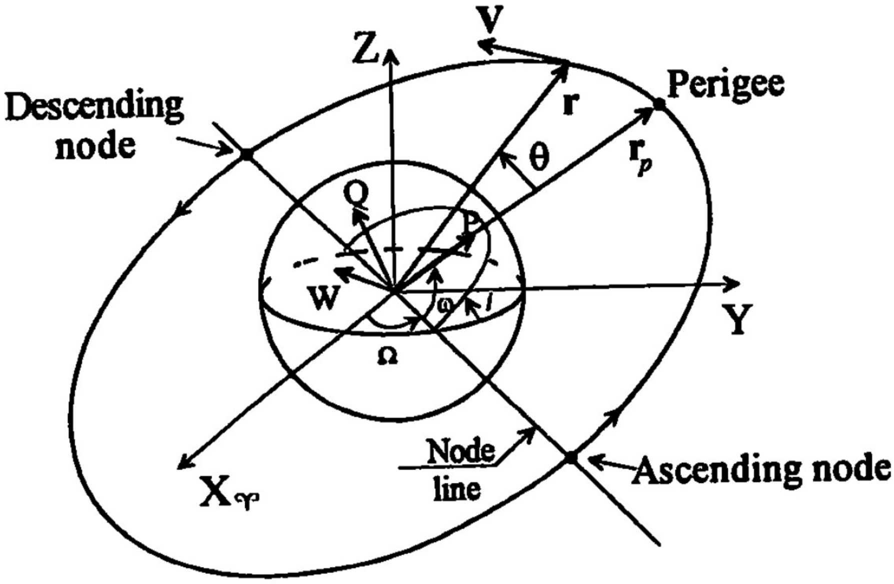

Figure 2.1: Classical Orbit Parameters (Sidi (1997))

2.3.3 Perturbed Orbits: Non-Keplerian Orbits

The orbit parameters are not constant and the derivative of each parameter can be written as functions that constitute the *Gauss planetary equations* when solved for arbitrary perturbing forces. When the perturbing forces considered for the Gauss equations are conservative, i.e. derived from a scalar function as $F_p = -\nabla U(r)$, the equations can be simplified to give the *Lagrange equations* for the differential change of the orbit parameters.

Earth-orbiting satellites have perturbed orbits predominantly from the difference of gravitational potential at different points of the orbit caused by the non-homogeneity and oblateness of the Earth. A third body, such as the sun or the moon, can cause further changes in the Keplerian orbit parameters, transforming to an n-body problem. The corresponding conservative perturbing forces which change the inclination of the orbit of geostationary spacecraft.

Non-conservative perturbing forces include solar pressure which cause changes to the eccentricity of the orbit, and atmospheric drag which decreases the major axis of the orbit, causing the spacecraft to deorbit. Solar pressure exerted by the sun in the form of solar radiation (electromagnetic waves) and solar wind (ionized nuclei and electrons) can be ignored in low orbits due to aerodynamic perturbing forces, but need to be considered in high-altitude orbits.

2.3.4 Perturbed Geostationary Orbits

Geosynchronous orbits are orbits whose orbital period are equal to the period of revolution of the earth about its own axis of rotation. A geostationary orbit is a geosynchronous orbit whose inclination is zero or close to zero and eccentricity is very small. The mission may require the satellite to be fixed in an apparent position with respect to the earth. The right ascension Ω of such equatorial orbits is ill-defined, due to which the orbit parameters are redefined as:

- a: the *semi-major axis* of the ellipse,
- $e_x = e\cos(\omega+\Omega)$ and $e_y = e\sin(\omega+\Omega)$ from the *eccentricity vector* $\boldsymbol{e}$,
- $i_x = i\cos(\Omega)$ and $i_y = i\sin(\Omega)$ from the *inclination vector* $\boldsymbol{i}$, and
- $l_m = M+\omega+\Omega-\theta_G(t)$: the *mean longitude*; i.e., the angular location of the satellite relative to the Greenwich meridian,

where $\theta_G(t)$ (Greenwich meridian siderial time) is angle between $\boldsymbol{X}_{\Upsilon}$ and the meridian, and the sidereal angle of the satellite is given as $\alpha = \Omega+\omega+\theta$.

2.3.5 Euler-Hill Equations

When two satellites move in almost identical orbits and are very near to each other, the coordinate frames of reference are chosen to be non-inertial, with the origin fixed at and moving with the center of mass of one satellite. The coordinates of the other satellite are calculated in this moving coordinate frame, hence describing the relative motion of satellites in neighboring orbits. These equations of motion of the second satellite with respect to the first are called the *Euler-Hill equations* or the *Hill equations*. This mechanism can be used to solve problems involving small perturbations (such as drag forces), the relative motion of neighboring satellites, and the rendezvous problem between two spacecraft.
Consider two satellites at radius vectors $\boldsymbol{r_1}$ and $\boldsymbol{r_2}$. We have $\boldsymbol{\rho} = \boldsymbol{r_1} - \boldsymbol{r_2}$. We know that $\ddot{\boldsymbol{r_1}} = -\mu\boldsymbol{r_1}/r_1^3$ and $\ddot{\boldsymbol{r_2}} = -\mu\boldsymbol{r_2}/r_2^3 + \boldsymbol{f}$, from which we get:

$$\ddot{\boldsymbol{\rho}} = \frac{\mu}{r_1^3}\left(-\boldsymbol{\rho}+3(\boldsymbol{r_1}\cdot\boldsymbol{\rho})\frac{\boldsymbol{r_1}}{r_1^2}\right)+\boldsymbol{f}+O(r^2) \implies \ddot{x}-2n\dot{y}-3n^2x = f_x, \ddot{y}-2n\dot{x} = f_y, \ddot{z}-n^2z = f_z$$

for the components of $\boldsymbol{\rho}$ and $\boldsymbol{f}$, where x and y are the plane distances between the two neighboring satellites, z is the off-plane distance, and n is the almost constant angular velocity of the reference orbit. Solving the first two dependent equations and the independent equation for z gives us the required relations between the two satellites. $x(t)$ and $z(t)$ are assumed to be small, while $y(t)$ is a part of an arc on the orbit in the direction of motion of the satellite.

2.4 Orbital Maneuvers

Almost always, a satellite is launched into the transfer orbit by a launch vehicle, following which it performs orbital maneuvers to reach the desired orbit. Orbits may be adjusted by single or multiple thrust impulses, of which the latter can effect any desired orbit change. Adjustments are done instead of placing it in the exact orbit to reduce fuel consumption and hence increase the capable weight for useful payload. During an orbit change, thrust is applied for some time. Due to the non-impulsive nature of thrust, some velocity is lost since the thrust direction during burns is not constant but rather angled with respect to the mean thrust direction.

2.4.1 Single-Impulse Orbit Adjustment

The velocity of a spacecraft at a perigee can be calculated as $V_p = \sqrt{2\left(\frac{\mu}{r_p} - \frac{\mu}{r_p + r_a}\right)}$. The altitude of perigee or apogee can be changed by using the velocity at perigee to calculate the required difference of velocities at two apogees. The spacecraft can similarly change the semi-major axis and the eccentricity at the apogee. However, there are limits on the values of semi-major-axis and eccentricity that can be achieved with single-impulse thrust adjustment. It is required that $2a_2 \geq r_1$ and $r_{p2} = a_2(1 - e_2) < r_1 < a_2(1 + e_2) = r_{a2}$ for the satellite to have a real value of velocity, where $\boldsymbol{r_1}$ is the radius vector of the point of impulse application.
Some communications satellite systems on elliptical orbits require to have an apogee footprint at a particular geographical latitude with an inclination of 63.435°. This requires a change in the argument of perigee ω, usually without varying the semi-major axis a and the eccentricity e, and hence keeping the orbit shape constant but rotating it in the orbital plane keeping the perigee point fixed. This is again achieved by calculating the required velocity difference, although the absolute value of velocities remain constant.

2.4.2 Multiple-Impulse Orbit Adjustment

Restrictions in modifying orbital parameters using a single impulsive thrust limits the initial and the final orbits to have at least one common point. This can be avoided using multiple-impulse orbit adjustments. Hohmann transfer between orbits allow transfer between circular orbits with minimum fuel consumption. This is equivalent to minimizing the total change in velocity, ΔV. This transfer is optimal as long as the ratio of the radius of the larger orbit to that of the smaller orbit is less than 11.8. It involves an intermediate transfer orbit, where the perigee lies on the smaller orbit and the apogee on the larger orbit. Assuming impulsive velocity changes, the total change in velocity is computed as the sum of the changes in velocity required for entering the transfer orbit from one circular orbit and leaving the transfer orbit into the other circular orbit. A similar mechanism is used to transfer from one elliptic orbit to another coplanar and coaxial orbit; i.e., impulses are applied at the perigee to enter and the apogee to leave the transfer orbit. Similarly, multiple-impulse orbit adjustments can be performed to maintain the altitude of low-orbit satellites. The semi-major axis a decreases due to atmospheric drag. The required change in velocity ΔV for an average disturbing drag force F_d is performed as $F_d \Delta t = m\Delta V = (m_i - m_f) g I_{sp} = \Delta m_{prop} g I_{sp}$ since the final mass $m_f = m_i(1 - \Delta V / g I_{sp})$.

2.4.3 Geostationary Orbits

The transfer of a geostationary satellite from GTO to GEO consumes fuel as much as approximately the dry weight of the satellite in one to four weeks, while the mission stage after reaching GEO of more than ten years consumes about 10% to 20% in ten years. Wasting 2% of fuel in the transfer equates to about a year loss in communications. Minimizing fuel consumption during orbital changes depends on the accuracy of delivering ΔV to the satellite. Since the GEO is a circular orbit on the equatorial plane, it is ideal to choose an equatorial launch site. When this is not possible, two tasks need to be achieved individually or simultaneously to reach GEO:

- *Zeroing the Inclination of the GTO*: This is equivalent to changing the spatial attitude of the orbit plane by the inclination i with all other parameters (including speed) fixed. With $V_f = V_i = V_a$ where V_a is the velocity at apogee, the change in velocity is given by the vector from $\boldsymbol{V_i}$ to $\boldsymbol{V_f}$; i.e. $\Delta V_1 = 2V_a \sin(i/2)$

- *Circularization of the GTO*: This task involves the spacecraft transferring from an elliptic orbit to a circular orbit, both meeting at the apogee. To raise the perigee altitude to geostationary orbit, a change of velocity is applied at the apogee as:

$$\Delta V_2 = V_{cir} - V_a = \sqrt{\frac{\mu}{r_{cir}}}\left(1 - \sqrt{\frac{2r_p}{r_{cir}+r_p}}\right)$$

- *Combined GTO-to-GEO Maneuver*: Two individual orbital changes spending a total of $\Delta V = \Delta V_1 + \Delta V_2$ is not fuel efficient. As a result, the two changes can be merged into a single ΔV stage: $\Delta V^2 = V_{GTO}^2 + V_{GEO}^2 - 2V_{GTO}^2 V_{GEO}^2 \cos i$

GTO-to-GEO orbital maneuvers are generally executed in more than one firing. This may cause attitude errors during the ΔV process, hence diverting the orbit of the satellite. A one-shot firing can equate to a loss of about 3.5 years of mission stage due to fuel consumption. ΔV is hence divided into two or more smaller ΔVs.

The parameters that change with time owing to perturbing forces are balanced by the *station keeping* (SK) of the geostationary orbit that predominantly consists of longitude (E-W) SK, inclination (north-south) SK, and eccentricity corrections. These corrections can be done by sequentially adding velocity components: ΔV_R along the radius vector, ΔV_N normal to the orbit plane, and ΔV_T tangential to the velocity vector. The parameter changes corresponding to the required velocity component along each axis is calculated and applied on the spacecraft.

Fuel budgets for satellites are determined based on the maneuvers from the transfer orbit to the final mission orbit and on the corrections required to stay in the mission orbit. This can be expressed in terms of ΔV, since the fuel mass to be expended depends on the initial mass of the satellite. The exact mass of required fuel depends on the year epoch and varies from spacecraft to spacecraft considering the various limits placed on the orbit parameters.

2.5 Attitude Dynamics and Kinematics

Consider a rigid body moving in space with a frame of reference whose origin coincides with the center of mass of the body. We know that $\boldsymbol{v}_i = \boldsymbol{v}_0 + \boldsymbol{\omega} \times \boldsymbol{r}_i$ and $\Delta T = 0.5v^2(\Delta m)$ from which we get the kinetic energy to be expanded to translational and rotational components as:

$T = \frac{1}{2}v_0^2 M + \frac{1}{2}\int(\boldsymbol{\omega} \times \boldsymbol{r}) \cdot (\boldsymbol{\omega} \times \boldsymbol{r})dm = T_{transl} + T_{rot}$ from which we get $T_{rot} = \frac{1}{2}\boldsymbol{\omega}^T[\boldsymbol{I}]\boldsymbol{\omega}$. Due to the complexity of equations arising from the non-diagonal terms of the inertia matrix, it is usually transformed into a diagonal one whose diagonals give the *principal moments of inertia*: I_x, I_y, and I_z. The moment of inertia about any instantaneous axis of rotation $\mathbf{1}_\xi$ is given as $I_\xi = a_x^2 I_x + a_y^2 I_y + a_z^2 I_z$, where $a_x = \frac{\omega_x}{\omega}$ and so on.
Euler's moment equation gives $\boldsymbol{M} = \dot{\boldsymbol{h}}_{\boldsymbol{I}} = \dot{\boldsymbol{h}}_{\boldsymbol{B}} + \boldsymbol{\omega} \times \dot{\boldsymbol{h}}$. For the principal axes of inertia, we get $M_x = I_x\dot{\omega}_x + \omega_y\omega_z(I_z - I_y)$ and so on, which are nonlinear equations without an analytical closed-form solution but can be solved under certain conditions such as axisymmetricity. On solving for asymmetric bodies about the principal axes where no external are applied, it can be found that angular motion is stable when the body is spinning about its axis of minimum (minor axis) or maximum (major axis) moment of inertia.

2.5.1 Nutation

Whenever the body $\boldsymbol{Z_B}$ axis deviates from the momentum vector $\boldsymbol{h}$, the angular velocity vector component $\boldsymbol{\omega}_{xy}$ rotates about $\boldsymbol{h}$ at the *nutation angle* θ, where $tan(\theta) = \frac{I_x}{I_z}tan(\gamma)$. The two vectors form two cones, the body cone and the space cone respectively. With h constant, if the body spins about the minor axis and there is some internal energy dissipation that tends to decrease the rotational kinetic energy to its minimum, the body will transfer the spin of rotation to the major axis. Hence, with non-zero energy dissipation, a spinning body is in stable angular motion only if it rotates about the major axis.

2.5.2 Motion of a Non-spinning spacecraft

Reference coordinate systems change for a spacecraft depending on the task that it is involved in during the given period of its life. We define a reference frame in which the spacecraft is to be three-axis attitude-stabilized. The *orbit reference frame* is one whose origin moves with the cm of the satellite. $\boldsymbol{Z_R}$ ('R' for 'reference') points toward the cm of the earth, $\boldsymbol{X_R}$ is in the direction of the velocity of the spacecraft in the plane of the orbit and perpendicular to $\boldsymbol{Z_R}$, and $\boldsymbol{Y_R}$ is normal to the local plane of the orbit and completes a three-axis right-hand orthogonal system. $\boldsymbol{\omega}_{RI}$ represents the angular velocity vector in this frame, relative to the inertial axis

frame. The *inertial axis frame* has its origin at the cm of the earth. The satellite's attitude with respect to a reference frame can be defined using a direction cosine matrix $[\mathbf{A}]$, by a quaternion vector $\mathbf{q}$, or by Euler angles (ϕ about $\mathbf{X}_B$, θ about $\mathbf{Y}_B$, ψ about $\mathbf{Z}_B$).
We need to know the angular velocities of the body axis frame wrt the reference axis frame and the velocity of the body axis frame wrt the inertial axis frame. From $\boldsymbol{\omega}_{BR} = p\boldsymbol{i} + q\boldsymbol{j} + r\boldsymbol{k}$ and $\boldsymbol{\omega}_{RI} = \omega_{RIx}\mathbf{1}_x + \omega_{RIy}\mathbf{1}_y + \omega_{RIz}\mathbf{1}_z$, we get $\boldsymbol{\omega}_{RI}$ expressed in the body frame as $\boldsymbol{\omega}_{RIB} = \omega_{RIBx}\boldsymbol{i} + \omega_{RIBy}\boldsymbol{j} + \omega_{RIBz}\boldsymbol{k}$, giving the angular velocity of the body frame wrt the inertial frame as $\boldsymbol{\omega}_{BI} = \boldsymbol{\omega}_{BR} + \boldsymbol{\omega}_{RIB}$. Here, $\boldsymbol{\omega}_{BR}$ helps us calculate the Euler angles of the moving body wrt any defined reference frame in space.
Axes transformations can be performed in any order. We consider three in particular: $\psi \to \theta \to \phi$ (rotation about $\boldsymbol{Z}_B$, then about the new $\boldsymbol{Y}_{B1}$, and then about $\boldsymbol{X}_{B2}$), $\theta \to \phi \to \psi$, and $\phi \to \theta \to \psi$. The former gives a direction cosine matrix as:

$$[\boldsymbol{A}_{321}] = [\boldsymbol{A}_{\psi\theta\phi}] = [\boldsymbol{A}_\phi][\boldsymbol{A}_\theta][\boldsymbol{A}_\psi]$$

which is the product of the three individual direction cosine matrices. The first rotation gives a derivative which is subject to all three rotations, the second to the latter two and the third to the last. As a result, the body angular rates, p, q and r can be computed by multiplying the corresponding direction cosine matrices to the derivative vectors and adding them. It can be noticed that the derivatives show a singularity at some particular angle for a rotation, such as $\theta = 90°$ for the first and the third transformation schemes and $\phi = 90°$ for the second, causing phenomena such as gimbal locks. This can be eliminated by using the quaternion terminology.
Given the initial direction cosine matrix $[\boldsymbol{A}(0)]$, we can find the time evolution of the direction cosine matrix by integrating

$$\frac{d}{dt}[\boldsymbol{A}] = [\Omega][\boldsymbol{A}] \text{ where } [\Omega] = \begin{bmatrix} 0 & \omega_z & -\omega_y \\ -\omega_z & 0 & \omega_x \\ \omega_y & -\omega_x & 0 \end{bmatrix}$$

. This integration is excessively time-consuming and instead the integration of the quaternion vector is more common. The corresponding differential equation for the quaternion system is given as

$$\frac{d}{dt}[\boldsymbol{q}] = \frac{1}{2}[\boldsymbol{\Omega}'][\boldsymbol{A}] \text{ where } [\boldsymbol{\Omega}'] = \begin{bmatrix} 0 & \omega_z & -\omega_y & \omega_x \\ -\omega_z & 0 & \omega_x & \omega_y \\ \omega_y & -\omega_x & 0 & \omega_z \\ -\omega_x & -\omega_y & -\omega_z & 0 \end{bmatrix}$$

.

In order to find the evolution of the Euler angles, we need to know $\omega_{BR} = \omega_{BI} - \omega_{RIB}$. ω_{BI} can be computed using inertial sensors such as precision rate integrating gyros. In order to find ω_{RIB}, we observe the reference frame coordinates as $\boldsymbol{k} = -\frac{\boldsymbol{r}}{|\boldsymbol{r}|}$, $\boldsymbol{j} = \frac{\boldsymbol{v}\times\boldsymbol{r}}{|\boldsymbol{v}\times\boldsymbol{r}|}$, and $\boldsymbol{i} = \boldsymbol{j} \times \boldsymbol{k}$. For a Keplerian orbit, we can see that a positive clockwise rotation δ about $\boldsymbol{j}$ gives us a $\boldsymbol{\omega}_{RI} = \left[0 \ \left(\frac{-1}{r^2|\boldsymbol{v}\times\boldsymbol{r}|}\boldsymbol{v}\cdot[(\boldsymbol{r}\cdot\boldsymbol{v})\boldsymbol{r} - (r^2\boldsymbol{v})]\right) \ 0\right]^T$, which, in a circular orbit simplifies to $\boldsymbol{\omega}_{RI} = [0 \ -\boldsymbol{j}\omega_0 \ 0]^T$ where $\omega_0 = \frac{v}{r}$.

2.5.3 Attitude Dynamics Equations of Motion for a Non-spinning Satellite

We consider the effect of *momentum exchange devices*, particularly the reaction wheel and the momentum wheel. Moreover, external inertial moments due to aerodynamic, solar, gravity or reaction torque factors contribute to the total external moment $\boldsymbol{M}$ acting on the body which is equal to the inertial momentum change of the system.
The external torque is given as $\boldsymbol{T} = \dot{\boldsymbol{h}}_I = \dot{\boldsymbol{h}} + \boldsymbol{\omega}\times\boldsymbol{h}$, where the momentum of the entire system is $\boldsymbol{h} = \boldsymbol{h}_B + \boldsymbol{h}_w$ consisting of the rigid body momentum $\boldsymbol{h}_B = [h_x \ h_y \ h_z]^T$ and the moment exchange device momentum $\boldsymbol{h}_w = [h_{wx} \ h_{wy} \ h_{wz}]^T$. $\boldsymbol{T}$ can be broken down as the control moments used to control the attitude motion $\boldsymbol{T}_c$ and the moments from disturbing environmental phenomena $\boldsymbol{T}_d$
The gravitational moment is inherent in low-orbit satellites. An asymmetric body subject to a gravitational field will experience a torque that tends to align the axis of least inertia in the direction of the field. Considering the force to be given as $\boldsymbol{R} = -R_0\boldsymbol{k}_R$ wrt the inertial axis, i.e. $[R_x \ R_y \ R_z]^T = [\boldsymbol{A}_{\psi\theta\phi}][0 \ 0 \ -R_0]^T$ wrt the body axes, and the gravitational force exerted on a mass element $d\boldsymbol{F} = -[(\mu dm)/|\boldsymbol{r}|^3]\boldsymbol{r}$ ($\boldsymbol{r} = \boldsymbol{R} + \boldsymbol{\rho}$ is the distance from the earth's cm to mass

dm), we get the gravity gradient vector as

$$\boldsymbol{G} = [G_x\ G_y\ G_z]^T = \frac{3\mu}{R_0^5}\int_M [\boldsymbol{R}\cdot\boldsymbol{\rho}][\boldsymbol{\rho}\times\boldsymbol{R}]dm$$

which on solving also gives $\boldsymbol{G}$ in terms of the direction cosine matrix elements. The hence obtained values for the G_x, G_y, and G_z can be linearized using small-angle approximations giving $G_x = 3\omega_0^2(I_z - I_y)\phi$, $G_y = 3\omega_0^2(I_z - I_x)\theta$ and $G_z = 0$ where $\omega_0 = \sqrt{\mu/R_0^3}$ is the angular orbital velocity of the body (*orbital rate* or *frequency*) in a circular orbit of radius R_0.
The relation given earlier between $\boldsymbol{\omega}_{BI} = \boldsymbol{\omega}_{BR} + \boldsymbol{\omega}_{RIB}$ and the Euler angles can be linearized for small Euler angles by linearizing the relation for $\boldsymbol{\omega}_{RIB}$ given $\boldsymbol{\omega}_{BR} = [p\ q\ r]^T$:

$$\begin{bmatrix}\boldsymbol{\omega}_{RIBx}\\ \boldsymbol{\omega}_{RIBy}\\ \boldsymbol{\omega}_{RIBz}\end{bmatrix} = \begin{bmatrix}1 & \psi & -\theta\\ -\psi & 1 & \phi\\ \theta & -\phi & 1\end{bmatrix}\begin{bmatrix}0\\ -\omega_0\\ 0\end{bmatrix} = \begin{bmatrix}-\psi\omega_0\\ -\omega_0\\ \phi\omega_0\end{bmatrix}$$

For small Euler angles, $p \approx \dot{\phi}$, $q \approx \dot{\theta}$ and $r \approx \dot{\psi}$, giving $[\omega_x\ \omega_y\ \omega_z] = [(\dot{\phi} - \psi\omega_0)\ (\dot{\theta} - \omega_0)\ (\dot{\psi} + \phi\omega_0)]$. The total external moment can be developed in terms of the Euler angles and other known values using this information. Here we consider the momentum components of reaction wheels with axes of rotation along the X_B, Y_B, and Z_B body axes which are expressed in terms of the moments of inertia and the angular velocities of the individual wheels. Attitude control of a spacecraft can be achieved by controlling the angular accelerations of the wheels which act as internal torques exerted on the satellite. External torques are also incorporated into the control torques. In general, reaction wheels need not be aligned to the body axes, and there may be more (or less) than three wheels, as a result of which their momenta and angular accelerations are transferred to the body axes.

2.6 Attitude Maneuvers in Space

2.6.1 Equations for Basic Control Laws

Several spacecraft require attitude maneuver as a primary mission task and this is formulated as control law equations expressed in different attitude error terminologies:

2.6.1.1 Using Euler angle errors

Given the Euler angles from s/c instrumentation, we have $T_{dx} + T_{cx} = I_x\ddot{\phi}$ [and similarly for y ($\ddot{\theta}$) and z ($\ddot{\psi}$)]. Hence, the control input can be written as $T_{cx} = K_x(\phi_{com} - \phi) + K_{xd}\dot{\phi}$, where ϕ_{com} and ϕ_E are the Euler command and error angles resp., and $\dot{\phi}$ is the Euler angular rate. This is simple to develop but will not be sufficient in large attitude maneuvers because of higher-order and cross-coordinate terms, saturation of control input and singularities at large Euler angle values (such as $\phi \to 90°$). Moreover, this control law gives an oscillating behavior with large attitude commands and the angular path of the Euler axis of rotation angle is large.

2.6.1.2 Using the Direction Cosine error matrix

Considering the present attitude of the spacecraft to be given by the direction cosine matrix $[\boldsymbol{A}_S]$ and that of the desired attitude as $[\boldsymbol{A}_T]$, the direction cosine error matrix is given as $[\boldsymbol{A}_E] = [\boldsymbol{A}_S][\boldsymbol{A}_T]^T$. This becomes the unit matrix when the two matrices are identical, meaning that the desired attitude has been achieved. Moreover, for the matrix to be diagonal, all diagonal terms should be equal to one and the other terms should be zeroed. Hence, a control law can be developed as $T_{cx} = K_x a_{23E} + K_{xd}p$ (similarly for y and z), where $a_{ijE} = -a_{jiE}$, and p is the angular velocity of the body axis in the reference frame (for damping). The error terms will be large in the beginning of the maneuver, but will approach the Euler angle errors when the s/c axes are aligned closer to the target axes.

2.6.1.3 Using the Euler Axis of Rotation

We can calculate the angle about the Euler axis of rotation as $cos(\alpha) = \frac{1}{2}[trace([\boldsymbol{A}_E]) - 1]$ which gives the control law $T_{cx} = -\frac{1}{2}K_x(a_{32E} - a_{23E}) + K_{xd}p$. Since a single axis is involved for rotation, the angular path is minimized. However, this law requires all six off-diagonal terms of $[\boldsymbol{A}_E]$ to be computed continuously.

2.6.1.4 Using the Quaternion error vector

Based on the present spacecraft attitude quaternion $\boldsymbol{q_S}$ and the desired attitude quaternion $\boldsymbol{q_T}$, an error quaternion can be defined as $\boldsymbol{q_E} = \boldsymbol{q_S}^{-1}\boldsymbol{q_T}$. There is a one-to-one equivalence between $[bmA_E$ and $\boldsymbol{q_E}$, based on which attitude control laws can be formulated as: $T_{cx} = 2K_x q_{1E} q_{4E} + K_{xd} p$ (similarly for y and z). Computing $\boldsymbol{q_E}$ requires fewer algebraic operations than computing $[bmA_E$, as a result of which the quaternion control law is preferred over the DCM control law. For large attitude maneuvers, with the quaternion control law, the Euler attitude angles are well-behaved and resemble their time responses for small attitude commands.

2.6.1.5 Body-Rate Estimation without Rate Sensors

It may not be possible to include or rely on rate gyro measurements for the three angular rates about the body axes of the spacecraft. In such scenarios, it will be required to estimate them from the knowledge of the quaternion vector or the DCM. This can be done by finding p, q, and r from $\dot{q}_i = \frac{1}{2}[\boldsymbol{Q}][p\ q\ r]^T, i = 1, ..., 4$, where $Q = \begin{bmatrix} q_{S4} & -q_{S3} & q_{S2} \\ q_{S3} & q_{S4} & -q_{S1} \\ -q_{S2} & q_{S1} & q_{S4} \\ -q_{S1} & -q_{S2} & -q_{S3} \end{bmatrix}$, using the left pseudo-inverse of $[\boldsymbol{Q}]$, $[\boldsymbol{Q}_L] = \left([\boldsymbol{Q}]^T[\boldsymbol{Q}]\right)^{-1}[\boldsymbol{Q}]^T$. Here, the quaternion vector is obtained in the first place using measurements from horizon, sun, or star sensors.

2.6.2 Control with Momentum Exchange Devices

A spacecraft can control attitude by applying torque generated using several mechanisms including earth's magnetic field, reaction forces produced by expulsion of gas or ion particles, solar radiation pressure on spacecraft surfaces, and momentum exchange devices (rotating bodies inside the s/c) such as reaction wheels, momentum wheels, and control moment gyros (CMGs). Using momentum exchange devices transfers angular momentum between different parts of the spacecraft without changing its overall inertial angular momentum. Particularly, reaction wheels provide very accurate attitude control systems with moderately fast but continuous and smooth maneuvers and very low parasitic disturbing torques.

Consider $\boldsymbol{h}_w = [h_{wx}\ h_{wy}\ h_{wz}]$ to be the momentum vector of all momentum exchange devices inside a spacecraft body with reference to the body axes. Any device's momentum change (say $\dot{h}_{wx}$) will produce an equal but opposite angular torque on the body about the corresponding body axis (here, $\boldsymbol{X_B}$). The required control torque command, $\dot{h}_{wx} = T_{cx} = K_x(\phi_{com} - \phi) + K_{xd}\dot{\phi}$ (similarly for y and z), is achieved by accelerating the rotor of electrical motors aligns with the body axes such that $\dot{h}_S + \dot{h}_w = 0$. The dynamics of the motors can be used to compute the voltage required to achieve this torque. Based on this concept, a control loop can be developed for attitude maneuvers. However, such a system cannot independently remove angular momentum that accumulates due to external disturbances.

Three reaction wheels aligned with the body axes are sufficient for independently controlling the spacecraft's attitude. However, this cannot be done if one of them becomes damaged. Hence, a geometrical configuration can be developed with four reaction wheels on the same plane parallel to the $\boldsymbol{X_B} - \boldsymbol{Y_B}$ plane, separated by 90° to the neighbors and inclined to the $\boldsymbol{X_B} - \boldsymbol{Y_B}$ by an angle β (to apply torques and momentum in the $\boldsymbol{Z_B}$ direction as well). For a given control vector $\hat{\boldsymbol{T}}_c$, the components T_i from each one of the four wheels i can be computed using the transformation between the three body axes' command control torques and the four wheels' command control torques as:

$$\begin{bmatrix} T_1 \\ T_2 \\ T_3 \\ T_4 \end{bmatrix} = \frac{1}{2} \begin{bmatrix} 1 & 0 & \frac{1}{2} & \frac{1}{2} \\ 0 & 1 & \frac{1}{2} & -\frac{1}{2} \\ -1 & 0 & \frac{1}{2} & \frac{1}{2} \\ 0 & -1 & \frac{1}{2} & -\frac{1}{2} \end{bmatrix} \begin{bmatrix} \hat{T}_{cx} \\ \hat{T}_{cy} \\ \hat{T}_{cz} \\ 0 \end{bmatrix}$$

Reaction wheels provide comparatively low parasitic disturbing torques. However, attitude sensors are no less responsible for the quality and attitude accuracy of the ACS. There are usually two dynamic states that need to be controlled: the attitude angle θ and the attitude stability $\dot{\theta}$. This control is done using attitude sensors and angular velocity sensors.

Earth sensors, though noisy, are the most common attitude sensor. Sun sensors are also common and are more accurate than earth sensors with lower statistical noise level. Star sensors are the most accurate attitude sensors but are very expensive and less reliable than earth and sun sensors with complex instrumentation and algorithms. Rate integrating gyros (RIGs) are the most common angular velocity sensors. They are very accurate and do not dependent on the s/c orientation in space. On the other hand, conventional rate sensors are less accurate and are used for rate sensing in control tasks such as rate control and damping in the ACS.

It is not possible to use earth sensors when the earth is outside the sensor's field of view, and star sensors are not useful during fast and large maneuvers. In such situation precise inertial measuring units (IMUs) such as RIGs are used. Some attitude position sensor such as a star sensor is required to accurately measure the initial conditions for the gyros' rate integration algorithm. It is also common for multiple attitude position sensors such as earth sensors along with a digital sun sensor to be used to initialize fast and large attitude maneuvers, although during the maneuver, the ACS utilizes the RIGs only.

It is possible to develop a control algorithm that integrates the attitude velocity from the RIG to find the attitude position. However, the sensor noise at very low frequencies can become the drift factor of the sensor, and without an actual attitude position sensor, this can lead to a divergent attitude position error. This drift term can be eliminated by further introducing a differentiator along with a first-order filter.

2.6.3 Magnetic Attitude Control

The earth's magnetic field interacts with a magnetic moment generated within a spacecraft to produce a mechanical torque acting on the spacecraft as:

$$\boldsymbol{T_B} = \boldsymbol{M} \times \boldsymbol{B}$$

where $\boldsymbol{M}$ is the generated magnetic moment inside the body and $\boldsymbol{B}$ is the earth's magnetic field intensity. In order to achieve a desired torque $\boldsymbol{T_c}$, it is required to find the magnetic moment vector $\boldsymbol{M} = [M_x\ M_y\ M_z]^T$. However, the cross-product matrix of $\boldsymbol{B}$ is singular and hence non-invertible. This can be solved by replacing a magnetic torqrod in one or two direction with reaction wheels.

There are a number of drawbacks to this method of control. First of all, the magnitude of earth's magnetic field is inversely proportional to the cube of the distance from its center as a result of which the magnetic moment should be drastically increased for the same amount of torque at a higher altitude. Secondly, the earth's magnetic field depends on orbit characteristics as well as on the location of the satellite within the orbit, especially on the inclination of the orbit. For example, the magnetic field for a polar orbit can be twice as strong as that of an equatorial orbit. And this dependence needs to be included in the control algorithm. Thirdly, the achievable levels of torques using magnetic torqrods are very limited and saturation limits are easily attained, as a result of which the control law can be extremely non-linear. However, the cost of a magnetic torqrod is typically one-tenth that of a reaction wheel, as a result of which such a configuration will be much cheaper than an ACS incorporating reaction wheels.

2.6.4 Magnetic Unloading of Momentum Exchange Devices

External disturbances acting on the body of an attitude-controller s/c induce accumulation of momentum in the momentum exchange devices leading to improper working conditions for the wheels. This excess momentum is unloaded when it exceeds some predetermined limiting value using magnetic torqrods and reaction thrusters. The basic control equation for momentum unloading is

$$\boldsymbol{T} = -k(\boldsymbol{h} - \boldsymbol{h}_N) = -k\Delta\boldsymbol{h},$$

where k is the unloading control gain, $\boldsymbol{h}$ is the wheel's momentum vector, $\boldsymbol{h}_N$ is the desired and nominal wheel momentum vector, and $(\boldsymbol{h} - \boldsymbol{h}_N) = \Delta\boldsymbol{h}$ is the excess momentum to be removed. k is obtained from trial-and-error due to the time-varying nature of the control system parameters, especially earth's magnetic field. The above equation is equated to $\boldsymbol{M} \times \boldsymbol{B}$, but since $\boldsymbol{M}$ cannot be directly computed, the equation is cross multiplied by $\boldsymbol{B}$ and it is assumed that $\boldsymbol{M} \perp \boldsymbol{B}$, giving

$$\boldsymbol{M} = -\frac{k}{B^2}(\boldsymbol{B} \times \Delta\boldsymbol{h}) \implies \boldsymbol{T} = -\frac{k}{B^2}(B^2\Delta\boldsymbol{h} - \boldsymbol{B}(\boldsymbol{B} \cdot \Delta\boldsymbol{h}))$$

No torque can be obtained about the earth's magnetic field as a result of which any excess momentum in this direction cannot be dumped. Fortunately, both the direction and the amplitude of $\boldsymbol{B}$ vary during most incline orbits and an average removal of the excess momentum can be performed although the efficiency of this operation dependent on the orbit (quite low for equatorial orbits).

2.6.5 Time-Optimal Attitude Control

Time-optimal control can be used to minimize the time of attitude orientation of the satellite in space. This is particularly useful for sky observation and earth-observing satellites that require to be oriented in a particular direction for a period of time. Transfer functions cannot be used since the controller is drawn into heavy saturation in order to deliver the maximum physically obtainable angular accelerations to the satellite. Satellite dynamics are usually characterized by a linear second-order plant and a nonlinear maximum-effort or on-off controller. Practical physical constraints such as control time delays, uncertainty in maximum control acceleration levels, and additional time constants from satellite hardware and structural dynamics need to be considered as well.

The basic time-optimal control about a single axis involves a bang-bang controller far from the origin while a linear controller is used close to the origin to avoid chattering. In practice, the activating torque T might be larger or smaller than the theoretical maximum torque T_{max} used in control equations. Owing to sampling and additional delays in the control loop, the solution will show an overshoot in the time-behavior if $T < T_{max}$ or a time delay Δt in the control loop resulting in a chatter along the switching line if $T > T_{max}$. To compensate for delays, switching commands need to be issued before when they are required based on the maximum time delay in the control loop.

The chapter primarily uses the reaction wheel assembly (RWA) in accurate and time-optimal attitude control. Choosing the wheel is dependent on the performance required by the ACS in terms of parameters such as maximum achievable torque, maximum momentum capacity, low torque noise, and low coulomb friction torques. If it is not possible to acquire the calculated parameters with existing commercial and space-qualified wheels, the specifications should be lowered, which will lead to an increase in the acceleration period and a prolongation in the time taken for attitude maneuvers.

Chapter 3

Basic Concepts on Formation Control

3.1 Introduction

A *multi-agent system* refers to a group of autonomous agents operating in a networked environment. This chapter presents the basic idea of decentralized multi-agent formation control. The methodologies involved in the corresponding algorithms are also presented. Agents are typically considered to be generic mathematical operators while some research consider them as physical objects such as spacecraft or satellites along with some level of consideration of their dynamic characteristics such as attitude and angular velocities.

3.2 Multi-Agent Collective Control

An individual system is controlled by its trajectory in the time dimension, denoted by $x(t)$ at time t. Knorn et al. (2016) depict multi-agent system as a two-dimensional model with system behavior $x_1(t,k)$ and network influence $x_2(t,k)$ at time t and agent index k. $n(t,k)$ denotes the

neighbors of agent k at time t, and $\tau(t,k)$ denotes the time of measuring this state.
System dynamics is analyzed in the time domain: $\delta x_1(t,k) = f(x_1(t,k), x_2(t,k), t, k)$ where δx_1 represents the continuous or discrete time derivative of x_1. System dynamics consist of plant dynamics and a designed controller, giving: $x_1(t,k) = [\xi^T(t,k), \zeta^T(t,k)]$, where $\xi(t,k)$ is the plant state and $\zeta(t,k)$ the controller compensator state. Meanwhile, the network influence is analyzed using the derivative with respect to k: $\Delta x_2(t,k) = g(x_1(\tau(t,k), n(t,k)), t, k) - x_2(t,k-1)$. The network influence does not usually propagate in the network dimension, hence eliminating $-x_2(t,k-1)$. The control design problem is to find suitable functions for the $\delta\zeta(t,k)$ such that $x_1(t,k)$ satisfies desired requirements in both dimensions.

3.2.1 Agent Dynamics

Agent dynamics can be segregated on the basis of the equations for the plant state. Research works have dealt with dynamics based on the linearity and homogeneity of agents.

3.2.1.1 Linear Homogeneous Network

The simplest case is a group of N identical single-integrator agents in continuous time given as $\frac{d\xi(t,k)}{dt} = u(t,k), k = 1,...,N$. The controller and the network influence are given as follows, where $a_{kj}(t)$ is the (k,j)-th element of the adjacency matrix $\mathscr{A}(t)$:

$$u(t,k) = x_2(t,k) = \sum_{j=1}^{N} a_{kj}(t)(\xi(t,j) - \xi(t,k))$$

This can be written in terms of the Laplacian matrix $\mathscr{L}(t)$ as: $\frac{d\xi(t)}{dt} = -\mathscr{L}(t)\xi(t), \xi(t) = [\xi(t,1),...,\xi(t,N)]$. This is described solely in the time dimension and not the network dimension. The controller causes the agents to present the collective behavior of consensus, whereby each agent converges towards the weighted average of the states of its neighbors. This can be generalized as $\frac{d\xi(t,k)}{dt} = A\xi(t,k) + Bu(t,k), y(t,k) = C\xi(t,k)$ where A, B and C are constant matrices of appropriate dimensions. Discrete-time systems have also been studied.
The state equation is given as $\frac{d\xi(t)}{dt} = \mathscr{L}\xi(t) + \mathscr{B}\mu(t)$, where $\mathscr{B}$ describes the influence of the external input onto $\xi(t)$. Reachability and controllability are based on the ability to control a subset of nodes $\mathbb{I}_c \subset 1,...,N$ by an external input $\mu(t)$ in addition to the local control input of

the consensus formation, whereas observability is based on the ability of an external processor that collects information from a subset of nodes $\mathbb{I}_o \subset 1,...,N$ to reconstruct the state of the entire network from $\eta(t) = \mathscr{C}\xi(t)$, where $\mathscr{C}$ relates the information gathered by the processor to $\xi(t)$. In the above model, $\mu(t)$ can be time-varying reference signals to the agents. The dynamic average consensus problem involves each agent tracking the average of individually measured reference signals. Contrarily, static consensus considers a snapshot of $\mu(t)$ to initialize the agent states following which it is ignored, resulting in the dynamic equation excluding $\mathscr{B}\mu(t)$.
Research on the robust stability of multi-agent systems has shown that one of the worst cases of perturbations is an identical diagonal perturbation. On testing single integrator networks achieving consensus for robustness to communication noise, it has been observed that systems with lower H_2 norms (Refer to Glossary) remain closer to the consensus despite the noise.

3.2.1.2 Linear Heterogeneous Network

There has been research on the *synchronization problem* by replacing the general values A, B and C with local state space representation A_k, B_k and C_k for describing the dynamics of agent k. The cooperative output regulation problem is formulated by subjecting this system to an exogenous signal $v(t)$ (reference input or disturbance) generated as $\dot{v}(t) = Sv(t)$:

$$\frac{d\xi(t,k)}{dt} = A_k\xi(t,k) + B_k u(t,k) + E_k v(t), y(t,k) = C_k\xi(t,k) + F_k v(t)$$

A distributed controller is designed that guarantees asymptotic stability for $v = 0$ and $y(t,k) = 0\ \forall k$. This is different from the general synchronization / consensus problem since the trajectory for each agent is defined by a real exosystem that acts as the leader that is followed by all subsystems of the plant. However, this method is unsuitable when investigating plant uncertainties. On the other hand, the virtual exosystem approach involves the heterogeneous version of the general synchronization problem. The controller is given as: $u(t,k) = H_k\zeta(t,k) + K_k x_2(t,k)$, $\frac{d\zeta(t,k)}{dt} = F_k\zeta(t,k) + G_k x_2(t,k)$, where $x_2(t,k) = P_k \sum_{j=1}^{N} a_{kj}(y(t,j) - y(t,k))$. Here, it is required for each individual system along with its local control to embed an internal model of the virtual exosystem $\dot{v}(t) = Sv(t)$ for synchronization.

3.2.1.3 Nonlinear Dynamics

There has been some research on complex networks such as scale-free or small world networks. However, complexity in synchronization problems have mainly arisen from nonlinear characteristics rather than network structures. Nonlinear MASs are more concerned with control design methodologies (possibly using nonlinear controllers) than conventional complex networks.
Velocity consensus and position consensus controllers have been proposed for networks of agents with nonlinear heterogeneous dynamics: $\frac{d\xi(t,k)}{dt} = \phi_k(\xi(t,k),t) + \psi_k(\xi(t,k),t)u(t,k)$, $y(t,k) = h_k(\xi(t,k))$. Previous research has mostly assumed the global Lipschitz condition (Refer to Glossary) or passivity, but some have designed nonlinear controllers for second-order systems without imposing these conditions. The synchronization problem for nonlinear heterogeneous systems described by the Euler-Lagrange equations has also been discussed.
The cooperative output regulation problem and the virtual exosystem approach have been developed for nonlinear systems as well. These involve a two-step manner involving the control of an individual agent to its reference model and the consensus of the reference models, hence permitting the internal model of each agent to be completely decentralized.

3.2.2 Network Topologies

Reaching consensus depends on the network topology for communications among agents, which is described using $n(t,k)$. The topology is fixed if $n(t,k)$ does not depend on t, switching if it varies with t taking values from a finite set, and time-varying if it varies with t otherwise.

3.2.2.1 Fixed Topologies

A network of single-integrator agents achieve consensus if the graph is connected (undirected network) or strongly connected and balanced (directed network). For a fixed topology with constant weights, consensus is achieved for a directed network of single-integrators or double-integrators if and only if the graph contains a spanning tree. Further research has dealt with cyclic graphs and cactus graphs (Refer to Glossary).

3.2.2.2 Switching Topologies

Switching topologies refer to non-fixed topologies where edges may be added or removed from the graph under varying circumstances, hence switching between elements of a finite set of graphs, contrary to time-varying topologies where an infinite set of arbitrary graphs is considered. Average consensus can be asymptotically achieved for a network of single-integrators with switching topologies taken from a finite collection of strongly connected and balanced digraphs. Research has further shown that consensus can be achieved if the union of the collection of interaction graphs over some time has a spanning tree frequently enough.

3.2.2.3 Time-varying Topologies

Agents following the 'nearest neighbor rule' interact with agents within a limited sensing radius, hence having an undirected graph topology. A discrete-time linearized network of such autonomous agents achieves consensus if the joint connectivity condition is satisfies; i.e., there exists an infinite sequence of continuous, non-empty and bounded time-intervals such that the union of the collection of graphs across each time interval is connected. The network achieves consensus regardless of switching as long as the graph remains connected. The problem of flocking has been studied using variants of the joint connectivity condition. Convergence, though not necessarily to consensus, can be achieved for cut-balanced time-varying topologies (Refer to Glossary). Time-variance of a network can also be caused due to active network weight tuning for which adaptive strategies can guarantee stability.

3.2.2.4 Leader-Follower Topology

Leader following involves following a particular agent ('leader') in the group with directed topology that does not have any incoming links. This is essential for distributed tracking control of MASs where the leader follows a reference trajectory. This problem has been solved using neighbor-based state-estimation, variable structure approach, etc. considering measurement noise, model uncertainties, delays and other non-ideal conditions. Consensus has been developed for single- and double-integrator networks based on 'pinning control' where only a small fraction of agents have access to the reference track. These agents act as leaders or are pinned by other leaders. Choosing the best set of pinned nodes is a problem of active research.

3.2.2.5 Preservation of Connectivity

A practical problem to deal with while satisfying different connectivity assumptions is how to preserve network connectivity. This can be done by defining a potential field such that the control algorithm forces the system to move along the negative of the slope to preserve network connectivity. This has been developed for centralized and distributed topologies, and has also been studied in mobile robotic networks as a part of network integrity (Refer to Glossary). Connectivity preservation is often studied with collision avoidance, where the control law combines a repulsive potential for obstacle avoidance and an attractive potential for convergence.
Previous research has developed navigation functions for single robots and multi-agent systems using potential fields for obstacle avoidance. Such navigation functions can work for stationary obstacles alongside maintaining global network connectivity or achieving an objective such as formation control or consensus. Externally applied boundary conditions can also be used to preserve connectivity preservation: a group of agents in a bounded plane can be almost always jointly connected and therefore form a complete flock.

3.2.3 Feedback and Communication

Feedback and communication mechanisms deal with modifications based on the measurement function g and/or the measurement time vector $\tau(t,k)$ of the network influence, where $x_2(t,k) = g(x_1(\tau(t,k),n(t,k)),t,k)$. Discretizing $\tau(t,k)$ represents sampled data control whereas discretizing g represents quantization. $\tau(t,k)$ can also be generalized to include communication delays.

3.2.3.1 Measurement Output Feedback Control

Very often, the actual state of an agent cannot be measured. Hence, measurement output feedback control is used usually with an observer design strategy. This problem has been solved using leader-follower systems as well as more general undirected topologies. Cases where only relative positions and not relative velocities are known to agents have been developed using connectivity preserving algorithms on switching topologies as well as the containment control problem (Refer to Glossary). Some research has also dealt with higher-order agents.

3.2.3.2 Sampled and Quantized Control

Realistic multi-agent systems send data at discrete time instances. This has been studied for fixed topologies and switching topologies, and necessary and sufficient conditions have been provided for coordination on the interaction graph, the damping gain and the sampling period. An allowable upper bound on the sampling period has been proposed for a network with random switching topologies. Moreover, due to bandwidth constraints, data is quantized before transmission. This has been studied for a quantized gossip algorithm, where at each time instant, exactly one agent updates its state based on the information transmitted from only one of its neighbors. Research has also been done on such systems for the average consensus problem.

3.2.3.3 Communication Delays

The exchange of information introduces delays between agents which, though usually ignored, have to be considered to study convergence towards consensus for an actual network of agents. Delays can predominantly be constant, time-varying, or distributed. Consensus in discrete-time systems has been shown for systems with arbitrary upper bounds on the delay with the graphs satisfying conditions such as being jointly rooted or the union over time having a spanning tree. Similar studies have been performed for continuous-time networks with finite delays. Identical integrators with heterogeneous delays converge to consensus against finite constant delays. Conditions for heterogeneous agents have also been developed.

3.2.4 Collective Behaviors

3.2.4.1 Formation Control

Formation control involves a group of agents moving through space along a desired reference trajectory while avoiding obstacles or other agents. A formation can be stabilized if and only if the sensor digraph is globally reachable. Previous research on this field includes: spacecraft formation control using leader following, behavioral approach, and virtual structure; formations using a group of point mass robots; and cyclic pursuit by unicycle agents around a common beacon with the same angular velocity and identical distances between neighboring agents. Multi-agent rendezvous where all agents have to meet at one point has been achieved, and formation shape control where agents achieve a desired shape and restore when perturbed. Here, graph rigidity should be considered if agents can actively control inter-agent distances.

3.2.4.2 Scalability of Networks

Scalability of networks can be a requirement in both the time and the network dimensions. Most research develops in the time dimension alone; however, the vehicle platoon (vehicle string) problem deals with the network dimension, wherein a group of N vehicles is required to follow a given reference trajectory while each one keeps a prescribed distance to neighboring vehicles. Although easily solvable in the time dimension, the propagation of error through the string (network dimension) results in a cumulative growth of error, referred to as 'string instability' or 'slinky effect'. This can be prevented in both unidirectional (information propagation in one direction) and bidirectional strings. Sufficient conditions have also proposed for scaling analysis and design tools with the network size, referred to as the 'scalable robust stability criterion'.

3.3 Multi-Agent Formation Control

Formation control is applicable in scenarios where there are several agents which are required to carry out a task in collaboration. Examples include GPS satellites which take positions such that any point on the surface can link to multiple satellites, and mobile robots which can together form a shape of interest. Oh et al. (2015) deal with formation control algorithms that are segregated on the basis of the sensing capability and the interaction topology of agents.

The terms *local* and *relative* are extensively used in formation control literature and can be described in terms of sensing capability and interaction topology as follows:

1. **Relative** is used to depict a variable when it is sensed with respect to a local coordinate system. The contrary involves sensing with respect to a global coordinate system and is termed as **absolute**.
2. **Local** is firstly used to depict an interaction topology where agents are not required to interact with all other agents. It is also used with respect to the sensing capability with a similar meaning as *relative*, hence implying the lack of a global coordinator.

Formation control can be generally divided into three major types: position-based, displacement-based, and distance-based. More general approaches have also been developed for the problem.

3.3.1 Position-based control

In a position-based control algorithm, all agents have global coordinates with respect to a global coordinate system. Though position control can be performed for individual agents, interactions among the agents may be beneficial. For example, given a first order control law, interactions such that the graph has a spanning tree can include additional control inputs due to which the absolute value of the eigenvalues of the error dynamics matrix increases.
Given the global agent coordinates $p_1, ..., p_N \in \mathbb{R}^3$, the objective is to move the agents from p_j to p_j^* for all j in $\{1, 2, ..., N\}$ (desired global coordinate) while satisfying $||p_j - p_i|| = ||p_j^* - p_i^*||$. Disturbances and actuator limitations prevent agents from perfectly tracking the trajectories. In such a scenario, the control system can use feedback coordination wherein agents are considered to form a rigid body, or virtual structure. The required optimization problem and corresponding desired trajectory can be solved by a global coordinator. Young et al. (2001) proposes a feedback coordination scheme where a coordinator gather performance data from individual spacecrafts and provides a coordination variable based on which the local coordinator gives a control input to the spacecraft. This has been proposed for unicycles as well by Beard et al. (2001).
Apart from these approaches, a state-space method has also been developed, for which using the absolute measurement (y_i) gives position-based control whereas using the relative measurement (z_i) gives displacement-based control:

$$\begin{cases} \dot{x}_i = A_p x_i + B_p u_i, \\ y_i = C_{p_a} x_i, \\ z_i = \sum_{j \in \mathcal{N}_i} C_{p_r}(x_i - x_j) \end{cases}$$

where $i \in \{1, 2, ..., N$, and x_i, u_i, y_i and z_i are the state, control input, absolute measurement, and relative measurement of agent i.

3.3.2 Displacement-based control

In displacement-based control, the orientations of agents are considered with respect to a global coordinate system. However, the origins for the agents are localized and different, and they need not know the global origin. The interaction topology can vary as per requirement but has to be connected and contain a spanning tree since the displacement of neighbors needs to be controlled. This form of control can be considered with numerous kinds of agents:

1. **Single-integrator modeled agents**: The control law is based on the single derivative of the displacement: $\dot{p}_i = u_i \forall i \in \{1, 2, ..., N\}$. Agents have individual local coordinate systems which are oriented with the global coordinate system. The displacement between the agents is maintained using the control law: $u_i = -k_p \sum_{j \in \mathcal{N}_i} w_{ij} \left((p_i - p_j) - (p_i^* - p_j^*) \right)$, where $w_{ij} > 0$ if an edge exists between agents i and j, $w_{ij} = 0$ otherwise, and $k_p > 0$.

2. **Double-integrator modeled agents**: The control law is based on the double derivative of the displacement, and for p_i, v_i and u_i being the displacement, the velocity and the control input of agent i respectively, the system follows:

$$\begin{cases} \dot{p}_i = v_i, \\ \dot{v}_i = u_i \end{cases} \forall i = 1, ..., N$$

   Relative velocities are controlled along with relative displacements (constants $k_p, k_v > 0$) as: $u_i = -k_p \sum_{j \in \mathcal{N}_i} w_{ij} \left((p_i - p_j) - (p_i^* - p_j^*) \right) - k_v \sum_{j \in \mathcal{N}_i} w_{ij} \left((v_i - v_j) - (v_i^* - v_j^*) \right)$.

3. **General linear agents**: The above cases can be generalized to a state-space model for N agents which can be modeled using LTI systems over a graph $\mathcal{G}$:

$$\begin{cases} \dot{x}_i = Ax_i + Bu_i, \\ y_{ji} = C(x_j - x_i), j \in \mathcal{N}_{ij} \end{cases}$$

   The system can provide a control input as: $u_i = KC \sum_{j \in \mathcal{N}_{ij}} w_{ij}(x_j - x_i)$ with the error defined as $e_x := x^* - x$. The desired formation is achieved if the graph contains a spanning tree and $A - \lambda_i KC$ is Hurwitz, where λ_i are non-zero eigenvalues of L.

4. **Nonholonomic modeled agents**: The case of unicycles on a plane is considered. Here, the position ($[x_i, y_i]^T$) and heading angle (θ_i) of each agent are known, and the control inputs are the linear (v_i) and angular velocities (ω_i) of each agent. Some algorithms achieve the desired formation with $\mathcal{G}$ being a spanning tree, while others require that $\mathcal{G}$ be connected and $(\mathcal{G}, \delta^*)$ is realizable (δ^* is the desired displacements for the formation). When $(\mathcal{G}, \delta^*)$ is not realizable, the agents may acquire a common velocity.

The agents may be required to move to a particular absolute position. In such a case, it will be required for some agents (number much smaller than total number of agents) to sense their absolute positions. To solve such a control problem, the control law will include a term which considers the error between the present and desired absolute positions. This can be extrapolated to linear systems where the control law will include a term which considers the error for the absolute state. This has been solved with a system where agents follow an acyclic directed interaction graph, where agents with no neighbors are leaders and sense their absolute positions, whereas others followers who compute their position based on the leader's position.
Scaling the formation can be achieved in a similar manner whereby the leader is made aware of a desired scaling factor λ^* which is subsequently sent to the followers or is estimated by the followers based on relative positions of their neighbors.

3.3.3 Distance-based control

In distance-based control, agents have independently-oriented local coordinate systems and their orientations are not dependent on other agents. If the interaction graph is not complete, the agents are required to achieve the desired formation by controlling partial inter-agent distances, and the interaction graph of the agents needs to be rigid or persistent. Rigidity is a measure by which the interaction graph of N agents is related to the completely connected graph of the N agents. An interaction graph is *rigid* if the inverse of the inverse of the edge function $g_{\mathscr{G}}(p) = \frac{1}{2}[...||p_j - p_i||^2...]$ for the graph and its completely connected equivalent graph lie in the neighborhood U_p. The interaction graph is globally rigid if the twice inverses are equal.
Similar to displacement-based control, agents can be modeled as single-integrators or double-integrators. The desired formation is described using the distances between the agents as E_{p^*}:

$$E_{p^*} := \{p \in \mathbb{R}^{nN} : ||p_j - p_i|| = ||p_j{}^* - p_i{}^*||, i, j \in \mathscr{V}\}$$

where $\mathscr{G} = (\mathscr{V}, \mathscr{E})$ and p^* represents the desired distances between the agents. This problem has been solved by using gradient descent on the local potential function for each agent as $\phi_i(p_i^i, ..., p_j^i, ...) := \frac{k_p}{2} \sum_{j \in \mathscr{N}_i} \gamma_{ij} \left(||p_j^i - p_i^i||\right)$, where $k_p > 0$ and $\gamma_{ij} : \mathbb{R} \rightarrow \bar{\mathbb{R}}_+$ is a differentiable function defining individual potentials. Though calculated for each agent individually, it is convenient to consider the agents in a global coordinate system for which a global potential

function is calculated and minimized using a globally computed gradient descent law.
The single-integrator model can have the control law $\dot{p} = u = -\nabla\phi(p)$. The desired formation is not globally asymptotically stable with respect to this system due to discrepancies at certain situations. This includes the case where all control inputs are zero or not defined since all the agents are at a common point, and the case where agents cannot escape from the line when they are all collinear. However, it has been shown that the control law allows agents to asymptotically approach desired 2D (triangular, equilateral triangular, etc.) and 3D formations.
Distance-based control of double-integrator modeled agents is done similar to displacement-based control. Here, the desired formation is given as:

$$E_{p^*,v^*} := \{[p^T v^T]^T \in \mathbb{R}^{2nN} : ||p_j - p_i|| = ||p_j{}^* - p_i{}^*, v = 0||, i, j \in \mathscr{V}\}$$

which requires speed to be zero along with the desired formation for the single-integrator model.
In contrast to the rigidity of an undirected interaction graph, a directed graph needs to be persistent for stability. Define p to be the positions assigned to the nodes. The position $p_i \in \mathbb{R}^n$ is said to be fitting for the desired squared distances d^*_{ij} if there is no $p'_i \in \mathbb{R}^n$ such that

$$\{æ \in \mathscr{N}_i\colon ||p_i - p_j||^2 = d^*_{ij}\} \subset \{æ \in \mathscr{N}_i\colon ||p'_i - p_j||^2 = d^*_{ij}\}$$

. Persistence is equivalent to rigidity along with a reasonable distribution of responsibility for the agents to control the inter-agent distances; i.e. a framework $(\mathscr{G}, p)$ is *persistent* if there exist a neighborhood of p such that every realization q fitting to p is congruent to p in the neighborhood. A minimally persistent framework is defined as a persistent framework whose persistence is lost on removing any edge. Distance-based control laws that assume persistence have to maintain stable rigidity by which the directed formation graph is acyclic and the underlying undirected graph is minimally rigid.

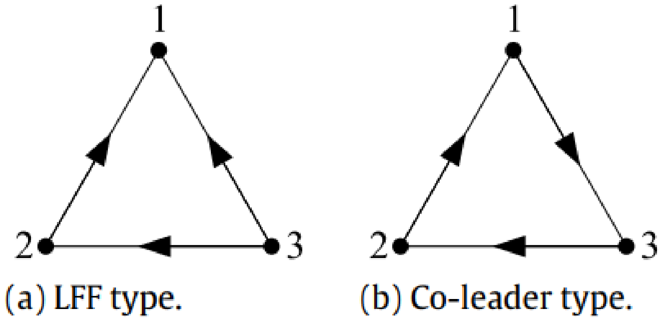

Figure 3.1: Minimally Persistent Formations (Oh et al. (2015))

Minimally persistent formations are either leader-first-follower (LFF), leader-remote-follower (LRF) or co-leader (depicted in Fig. 3.1). Studies on triangular LFF and co-leader formations have shown that the agents can exponentially converge to the desired formation as long as the initial positions of the three agents are not collinear. Followers can maintain the desired formation when the leader is traversing slowly along the reference trajectory. However, unless the leader is stationary, the formation will be erroneous. To prevent this, followers may move according to an estimated position of the leader.

3.3.4 Other approaches and correction techniques

Since several collective behaviors are based on relatively simple interactions between individuals, a generic agent model can be developed such that it satisfies Reynolds' rules, given as:

1. *Cohesion*: stay close to nearby neighbors
2. *Separation*: avoid collisions with nearby neighbors
3. *Alignment*: match velocity with nearby neighbors

Several control laws have been developed following this model that study the single-integrator and double-integrator modeled agents on planes and n-dimensional space.
The measurements taken for positions, displacements or distances need not be exact due to erroneous sensor readings. This can be solved by estimating the actual value p_i as $\hat{p}_i$. This estimate gives us an error of $\tilde{p}_i = p_i - \hat{p}_i$. For single-integrated models following position-based control, $\hat{p}_i$ asymptotically converges to p_i up to translation if $\mathscr{G}$ is uniformly connected.
A formation shape control scheme can be developed where purely distance-based control is

performed; i.e. only inter-agent distances are considered for computing relative positions of neighbors. This scheme repeatedly divides the agents in (at most four) subgroups and reduces the local potential functions one subgroup at a time. Globally asymptotic stability to a desired formation has been achieved using angle-based control as well, where the desired formation is represented in terms of angles $\alpha^* = [\alpha_1^* \; \alpha_2^* \; \alpha_3^* \; ...]^T$.

Containment control problems consist of follower agents which are driven into the convex hull spanned by leader agents based on consensus, and is effective is avoiding expensive sensors. On the other hand, cyclic pursuit problems consist of agents that follow their next agents (agent i follows agent $(i+1)\%N$), such that equilibrium formation is a generalized regular polygon.

3.4 A Planar Three-Coleader Formation Control problem

Previous research has dealt with formation control based on inter-agent distance preservation. Anderson et al. (2007) consider controlling the distance between two agents in a directed manner, by assigning it to only one of the two agents. This is trivial if the directed graph hence developed is acyclic since followers are influenced by leaders but not the other way. Considering cyclic structures for distance-based control cause more complicated problems than acyclic ones; however, balanced directed graphs can effectively solve the control problem. This paper considers the simplest two-dimensional formation with a simple balanced graph.

3.4.1 The Problem

The problem involves three holonomic massless point agents each with one degree of freedom, placed initially at incorrect distances from each other. Agent i knows the current distance (r_i), the required distance (d_i) and the direction of the next agent $i+1$. It is assumed that:

- the triangular inequality $d_i + d_j > d_k$ holds for $i \neq j \neq k$, and
- no two agents coincide in their position.

These two assumptions cause angles α_i to be well-defined throughout the motion even when the agents are collinear. The entire system can be visualized as follows:

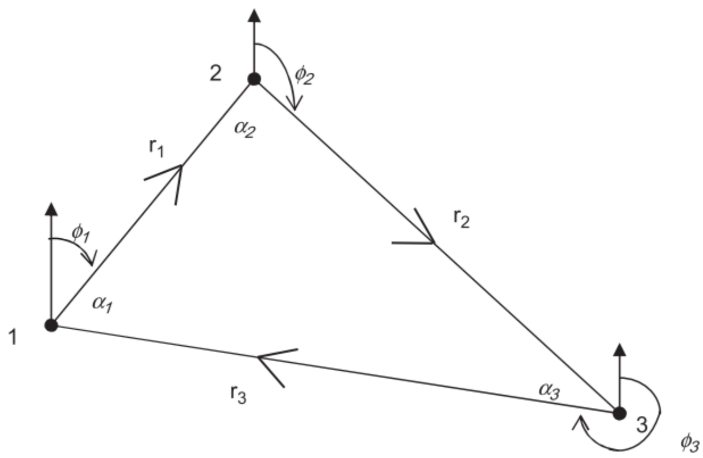

Figure 3.2: Three-Coleader Formation (Anderson et al. (2007))

3.4.2 The Solution

The control law initially aims to converge the present distances to the required distances and defines the speed of agent i as $s_i = -(d_i - r_i)$. This gives the speeds in individual coordinates as $\dot{x}_i = s_i sin(\phi_i)$ and $\dot{y}_i = s_i cos(\phi_i)$, and the angles as $\alpha_i = cos^{-1}\left(\frac{r_{i-1}^2+r_i^2-r_{i+1}^2}{2r_{i-1}r_i}\right)$. However, since the motion of agent i towards or away from agent $i+1$ changes the its direction with respect to agent $i-1$, the system also requires a control law to govern the angle between agents.
From the figure, we observe that $\phi_i = \phi_{i-1} + (\pm\pi - \alpha_i)$ such that $\sum\alpha = \pi$. Based on the initial control law, the existence of a solution and asymptotic stability can be proven from error dynamics based on the error variables $e_i = r_i - d_i$. The solutions are well-defined as long as no r_i is zero throughout the solution trajectory. The error dynamics can be calculated as:

$$\begin{bmatrix} \dot{e}_1 \\ \dot{e}_2 \\ \dot{e}_3 \end{bmatrix} = \begin{bmatrix} -1 & -cos(\alpha_2) & 0 \\ 0 & -1 & -cos(\alpha_3) \\ -cos(\alpha_1) & 0 & -1 \end{bmatrix} \begin{bmatrix} e_1 \\ e_2 \\ e_3 \end{bmatrix}$$

This gives us four equilibrium points: $[0,0,0]^T$, $k_1[-1,-1,1]^T$, $k_2[1,-1,-1]^T$ and $k_3[-1,1,-1]^T$, where $k_1 = (d_1+d_2-d_3)/3$, $k_2 = (-d_1+d_2+d_3)/3$ and $k_3 = (d_1-d_2+d_3)/3$, of which none give $r_i = 0$; i.e. $e_i = -d_i$, as long as the first assumption of triangular inequality holds true. This gives us three invariant motions of the system trajectory where the three agents are collinear.
Based on the dynamics and the previously proposed control law, we obtain a relation that gives

the corresponding control law for angular motion: $\dot{\phi}_1 = r_1^{-1}(r_2 - d_2)sin(\alpha_2)$, by which r_i will converge exponentially to d_i. Hence, although the differential equation for ϕ_i is not asymptotically stable, the variable will converge to zero since it depends on $d_i - r_i$ which decays exponentially to zero. Due to this exponential stability, the error e_i will converge to some neighborhood of zero in the presence of noise or bias. However, the formation may end up rotating or translating with a constant velocity. To prevent this, an external input determining the requirement to move or rotate can be supplied to the system. Also, deadzones can be introduced that will prevent this issue for larger error or bias although the error may not converge exactly to zero.

Chapter 4

Practical Applications of Decentralized Formation

4.1 A Multi-Agent Coordination problem using Distributed Pattern Matching

Sakurama et al. (2019) develop upon a problem of multi-agent distributed formation control where the agents aim to achieve a final shape, possibly after rotation by $R(t)$ and translation by $\tau(t)$, hence giving the control objective: $\lim_{t\to\infty}(x_i(t) - (R(t)x_{*i} + \tau(t))) = 0$ where $x_i(t) \in \mathbb{R}^d$ is the current position of agent $i \in \{1,2,...,n\}$ in the global frame and $x_{*i}(t) \in \mathbb{R}^d$ is its position in a desired formation. This can be solved using attitude synchronization at the cost of exchanging information about $R_i(t)$ and $\tau_i(t)$, and using a distance-based formation control using only relative positions and local bearings at the cost of solving for equally possible but unexpected formations (such as the reflection of a point through another).

To avoid these drawbacks, the problem can be directly solved by considering the control objective as an optimization problem, and solving for $R(t)$ and $\tau(t)$ to best match x_{*i} to $x_i(t)$. Formation control is performed using relative positions and local bearings via distributed pattern matching executed over each clique of networks in order to achieve the best control performance in attaining the desired configuration. The concept of *clique rigidity* gives a necessary and sufficient condition for the network being capable of achieving the configuration.

4.1.1 The Problem

A group of n mobile agents is considered in a d-dimensional space, indexed by $\mathscr{V} = 1, 2, ..., n$. Transfer of information can happen between two agents i and j only if they are neighbors on the graph $\mathscr{G} = (\mathscr{V}, \mathscr{E})$; i.e., there exists an edge between them. Agent positions are defined by a fixed and common global frame Σ, and a time-varying local frame $\Sigma_i(t)$ that is translated and rotated from Σ by $x_i(t)$ and R_i respectively. The dynamics of agent i is given as $\dot{x}_i(t) = R_i u_i(t)$ for a control input $u_i(t) \in \mathbb{R}^d$. Agent i can measure the relative position of a neighbor $j \in \mathscr{N}_i$ in $\Sigma_i(t)$ as $x_j^{[i]}(t) = R_i^T(x_j(t) - x_i(t))$ and the control input is computed as $u_i(t) = f_i\left(\left[x_j^{[i]}(t)\right]_{j\in\mathscr{N}_i}\right)$
The control law aims to converge the distances between the actual positions and the desired positions of agents to zero: $\lim_{t\to\infty} \text{dist}(X(t), \mathscr{T}_{X_*}) = 0$ where $\mathscr{T}_{X_*} = \{X \in \mathbb{R}^{d\times n} \colon \exists(R, \tau) \in SE(d)$ s.t. $X = RX_* + \tau\mathbf{1}_n^T\}$ is the target set of the collective position $X(t) = [x_1(t), x_2(t), ..., x_n(t)]$, and $X_* = [x_{*1}, x_{*2}, ..., x_{*n}]$ is the collective desired position.
A gradient flow approach can be used by which a function v (with minimum value zero) evaluates the achievement of a given task. From $\dot{x}_i(t) = -\frac{\partial v}{\partial x_i}(X(t))$, we observe that $v(X(t))$ should be monotonically non-increasing, and that $X(t)$ locally converges to the zero set $v^{-1}(0)$. Also, $u_i(t) = -R_i^T \frac{\partial v}{\partial x_i}(X(t))$. Hence, we need to find $v(X)$ with $v^{-1}(0) = \mathscr{T}_{X_*}$ ($v(X)$ becomes an *indicator* to $\mathscr{T}_{X_*}$) to detect whether the desired formation has been achieved. Here, $v(X) \in \mathscr{F}_r \cap \mathscr{F}_d(G) \cap \mathscr{F}_0(X_*)$ for a sufficient quantity of edges of graph G, where $\mathscr{F}_r(G)$ and $\mathscr{F}_d(G)$ are the set of all continuous functions having relative gradients and distributed gradients over G respectively. We need to minimize the Hausdorff distance (Refer to Glossary) between $v(X)$ and $\mathscr{T}_{X_*}$ to find the *best approximate indicator* (BAI); i.e. min[H-dist($v(X) - (\mathscr{T}_{X_*})$].

4.1.2 The Solution

The multi-agent coordination problem can be solved using the concept of pattern matching. A rigid body in a d-dimensional space is represented by a sequence of m points in $\mathbb{R}$: $y_1, y_2, ..., y_m$ in Σ_y, and $z_1, z_2, ..., z_m$ in Σ_z, such that $y_i = Rz_i + \tau$ with rotation matrix $R \in \mathrm{SO(d)}$ and translation vector $\tau \in \mathbb{R}^d$. Pattern matching can be used to minimize the total sum of the square errors; i.e., $\min_{(R,\tau)\in\mathrm{SE(d)}} ||Y - (RZ + \tau\mathbf{1}_m^T)||^2$ where $Y = [y_1\ y_2\ ...\ y_m] \in \mathbb{R}^{d\times m}$ and $Z = [z_1\ z_2\ ...\ z_m] \in \mathbb{R}^{d\times m}$. Consider the singular value decomposition (SVD): $(Z - ave(Z)\mathbf{1}_m^T)(Y - ave(Y)\mathbf{1}_m^T)^T = USV^T$ with orthogonal matrices $U, V \in \mathbb{R}^{d\times d}$ and diagonal matrix $S = \mathrm{diag}(\sigma_1\ \sigma_2\ ...\ \sigma_m)$ (σ_i are the singular values). The solution for the minimization problem is $R = V\ \mathrm{diag}(1, ..., 1, \det(UV))U^T$ and $\tau = ave(Y - RZ)$. If a unique solution is not obtained for U and V, a set-valued function $\mathscr{R}_m$ is considered such that all $R \in \mathscr{R}_m$ satisfy the above relation.

The function $v(X)$ has a distributed gradient (Refer to Glossary) only if it can be decomposed as a sum of continuous and differentiable functions with each function dependent on $[x_j]_{j\in\mathscr{C}}$ for each clique $C \in M - clq(G)$. For graph G and the target set $\mathscr{T}_{X_*} \subset \mathbb{R}^{d\times n}$, a BAI to $\mathscr{T}_{X_*}$ is given as:

$$v(X) = \sum_{\mathscr{C}\in M-clq(G)} \frac{\alpha_{\mathscr{C}}}{2} \left[\mathrm{dist}([x_j]_{j\in\mathscr{C}}, \mathscr{P}_{\mathscr{C}}(\mathscr{T}_{X_*}))\right]^2$$

where $\alpha_{\mathscr{C}} > 0$, and $\mathscr{P}_{\mathscr{C}}(\mathscr{T}_{X_*})$ is the projection of $\mathscr{T}_{X_*}$ onto the $[x_j]_{j\in\mathscr{C}}$ space; i.e., $\mathscr{P}_{\mathscr{C}}(\mathscr{T}_{X_*}) = \{Y \in \mathbb{R}^{d\times|\mathscr{C}|} : \exists(R,\tau) \in \mathrm{SE}(d) \text{ s.t. } Y = R[x_{*j}]_{j\in\mathscr{C}} + \tau\mathbf{1}_{|\mathscr{C}^T|}\}$. This reduces to the optimization problem of minimizing the total sum of the square errors and can be solved using pattern matching. The gradient-based control input with $v(X)$ is obtained as:

$$u_i(t) = \sum_{\mathscr{C}\in \text{M-clq}_i(G)} \alpha_{\mathscr{C}} \left[\mathrm{ave}\left([x_j^{[i]}(t)]_{j\in\mathscr{C}}\right) + R_{\mathscr{C}}(t)\left(x_{*i} - \mathrm{ave}([x_{*j}(t)]_{j\in\mathscr{C}})\right)\right]$$

4.2 Decentralized Spacecraft Formation Flying using a Virtual Structure

Ren and Beard (2004) compare three forms of formation control. First of all, the leader-follower approach has been adopted in previous research where leaders follow predefined paths and followers track the states of neighbors based on this motion. This is simple and easy to implement, however it can cause issues due to the leader being a single point of failure and the formation not being maintained when followers are perturbed in the absence of formation feedback. Secondly, the behavioral approach considers a control algorithm based on the weighted average of the control for the desired behaviors of the agent. Being a decentralized implementation, this is a robust and reliable mechanism. However, it is difficult to mathematically analyze such a system and it is not capable of maintaining the formation during maneuvers. Thirdly, the virtual structure approach considers the entire formation as a single body. This satisfies the conditions of the problem statement in the paper that: the framework should be decentralized since it involves a large number of agents, formation feedback should be used to improve robustness, the formation should be easily maneuverable, and the framework should be maintained with high precision during maneuvers. Previous research has dealt with a centralized architecture using the virtual structure approach. Here, a discrete event supervisor $\mathbf{G}$ provides the current formation pattern to a formation control module $\mathbf{F}$. $\mathbf{F}$ produces and broadcasts the coordination vector $\boldsymbol{\xi}$ which is converted by a local controller $\mathbf{K}_i$ to the desired state for the local spacecraft $\mathbf{S}_i$. $\mathbf{S}_i$ finally converts this state to the control input $\mathbf{u}_i$. Since $\mathbf{G}$ and $\mathbf{F}$ is centralized at the first spacecraft, heavy communications load can deteriorate the overall performance of the system. Moreover, the centralized node can act as a single point of failure for the whole system.

Decentralized control has also been previously research wherein a bidirectional ring topology is used for communication of state information. The robots are moved to their final destinations while maintaining the formation during transition. Other research have also dealt with maintaining zero attitude error and rotating the spacecraft about a defined axis of rotation.

4.2.1 The Problem

The paper presents a decentralized approach where the formation designs the coordination vector such that agents are connected in a bidirectional ring topology. Contrary to the centralized approach, each agent has a local copy of the discrete event supervisor as $\mathbf{G}_i$ and of the formation controller as $\mathbf{F}_i$ alongside $\mathbf{K}_i$ and $\mathbf{S}_i$. The state $\boldsymbol{\xi}_i$ is computed based on $\boldsymbol{\xi}_{i-1}$ and $\boldsymbol{\xi}_{i+1}$. This is shown in Fig. 4.1. Formation feedback can also be included from other agents at the cost of additional computation.

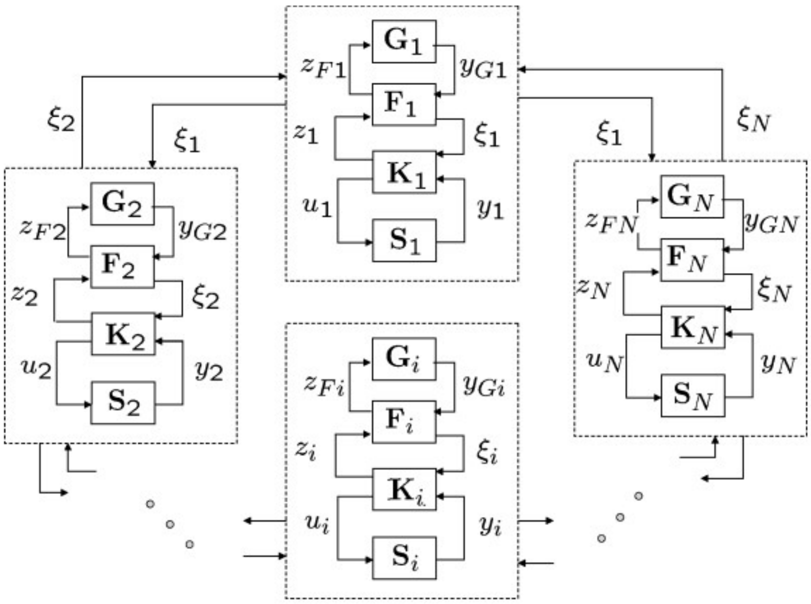

Figure 4.1: Decentralized Formation using Virtual Structure Approach (Ren and Beard (2004))

4.2.2 The Solution

Control laws are proposed, first for the spacecraft to follow the desired states prescribed by the virtual structure, and then for each virtual structure instantiation to synchronize to achieve the desired formation pattern. Finally the solution provides a convergence analysis for the system with the coupled dynamics of N spacecrafts with N coordination vector instantiations.

Firstly, the actual physical state of the spacecraft is defined as $\mathbf{X}_i = [\mathbf{r}_i^T, \mathbf{v}_i^T, \mathbf{q}_i^T, \boldsymbol{\omega}_i^T]$, the desired state as $\mathbf{X}_i^d$ and the error state as $\tilde{\boldsymbol{X}}_i = \mathbf{X}_i - \mathbf{X}_i^d$. The proposed control force and torque is developed from the state and its derivative. A control law is further proposed for the ith coordination vector instantiation $\boldsymbol{\xi}_i$. The current desired constant goal is given as $\boldsymbol{\xi}^{d(k)}$, simplified as $\boldsymbol{\xi}^d$, and the error state is given as $\tilde{\boldsymbol{\xi}}_i = \boldsymbol{\xi}_i - \boldsymbol{\xi}^{d(k)}$. The control law uses behavior-based strategies to evolve the instantiation to the desired goal ($\boldsymbol{\xi}^d$) as well as synchronize each instantiation ($\boldsymbol{\xi}_1 = \boldsymbol{\xi}_2 = ... = \boldsymbol{\xi}_N$). Two errors are defined: E_G as the goal-seeking error represented by the total error between $\boldsymbol{\xi}_i$ and $\boldsymbol{\xi}^d$, and E_S as the synchronization error represented by the total synchronization error between neighboring instantiations. The control objective is to asymptotically drive the total error $E(t) = E_G(t) + E_S(t)$ to zero.

To incorporate formation feedback into the system, $\Gamma_{Gi} = D_G + K_F e_{Ti}$ is defined where D_G and K_F are symmetric positive definite matrices and $e_{Ti} = ||\tilde{X}_i||^2$ represents the tracking performance for the ith spacecraft. The proposed control force and control torque are given as:

$$\boldsymbol{f}_{Fi} = m_F \left(-K_G(\boldsymbol{r}_{Fi} - \boldsymbol{r}_F^d) - \Gamma_{Gi}\boldsymbol{v}_{Fi} - K_S(\boldsymbol{r}_{Fi} - \boldsymbol{r}_{F(i+1)} + \boldsymbol{r}_{Fi} - \boldsymbol{r}_{F(i+1)}) - D_S(\boldsymbol{r}_{Fi} - \boldsymbol{r}_{F(i+1)} + \boldsymbol{r}_{Fi} - \boldsymbol{r}_{F(i-1)})\right)$$

$$\boldsymbol{\tau}_{Fi} = -k_G \widehat{\boldsymbol{q}_F^{d*}\boldsymbol{q}_{Fi}} - \Gamma_{Gi}\boldsymbol{\omega}_{Fi} - k_S(\widehat{\boldsymbol{q}_{F(i+1)}^{*}\boldsymbol{q}_{Fi}} + \widehat{\boldsymbol{q}_{F(i-1)}^{*}\boldsymbol{q}_{Fi}}) - D_S(\boldsymbol{\omega}_{Fi} - \boldsymbol{\omega}_{F(i+1)} + \boldsymbol{\omega}_{Fi} - \boldsymbol{\omega}_{F(i-1)})$$

where K_G is a symmetric positive definite matrix, K_S and D_S are symmetric positive semi-definite matrices, $k_G, k_S > 0$ are scalars, and $\hat{\boldsymbol{q}}$ represents the vector part of quaternion $\boldsymbol{q}$.

The formation may expand or contract along each $\mathscr{F}_F$ axis with the vector $\boldsymbol{\lambda}_F = [\lambda_1, \lambda_2, \lambda_3]$. A control law similar to that for force and torque can be developed for the virtual control effort $\boldsymbol{\nu}_{Fi} = \ddot{\boldsymbol{\lambda}}_{Fi}$ as well. The first two terms in the equations for $\boldsymbol{f}_{Fi}$, $\boldsymbol{\tau}_{Fi}$ and $\boldsymbol{\nu}_{Fi}$ drive $E_G \to 0$, and the others synchronize neighboring coordination vector instantiations. Moreover, the second terms (formation feedback term) slow down the implementation when tracking error is large.

For the control laws for the spacecrafts and the coordination vector instantiations, $\sum_{i=1}^N e_{Ti} + E(t) \to 0$ asymptotically. This can be proven using the stability of a suitable Lyapunov function, followed by application of lemmas described in the paper and LaSalle's invariance principle. This theorem proves that the formation maneuver is achieved asymptotically.

4.3 Robotic Assembly of a Modular Space Telescope

She and Li (2020) investigate and solve the problem of assembling a large space telescope in orbit. The solution utilizes space robots to join parts of the telescope rather than each part performing self-assembly using formation control. The paper deals with two sub-problems, the first being the mapping between the assembly path and the assembled piece number, and the second being a two-level hybrid optimization algorithm inspired from previously used algorithms.

4.3.1 The Problem

Constructing a structure in space can be done using two broad schemes: the first involves human involvement in the assembly (eg: International Space Station), and the second involves autonomous in-orbit assembly. Autonomous assembly can further be sub-divided as assembly using a servicing platform and space manipulators, and assembly by formation flying and docking maneuver. The former method is considered since the latter involves drawbacks such as high collision risk, large fuel consumption and high requirement for a GNC system.

The problem involves the construction of a 60-meter parabolic space telescopic mirror using 274 hexagonal pieces and six working regions (R_1 to R_6). Previous research has dealt with similar problems with single robots for mission planning and feasibility analysis. However, since the required structure is reasonably large, mission assignment, planning and scheduling are dealt with for multiple robots. More constraints arise from the fragility of telescope mirrors. Odd (and even) regions are identical and symmetric about the z-axis, with 49 (44 for even) pieces assigned to each region. The telescope's parabolic surface is described by $z(i) = a \cdot (\sqrt{x(i)+y(i)})^{\gamma}$ where a and γ are positive constant coefficients. The problem involves developing an optimization algorithm to minimize the time for assembly and hence the distance traveled by each robot. The assembly paths are considered to be symmetric, with all odd assembly paths being rotated copies of the first and similarly so for even assembly paths. Moreover, the problem assumes that the base requires connection to the telescope structure and that its dynamic effect is negligible due to the huge mass of the structure.

4.3.2 The Solution

The optimization problem imposes specific conditions: an already assembled piece should not be revisited to minimize the risk of damage to the reflector, and all pieces should be assembled by the final time-step in the algorithm. This problem can be solved using existing solvers such as the Genetic Algorithm (Refer to Glossary), and due to symmetry, the optimization problem needs to be solved only for R_1 and R_2, beyond which the same solution is adopted for all manipulators.

The work space of a manipulator is the area that can be reached by its end-effector. More realistically, the work space of the base located at a particular piece is defined as the the pieces connected to that piece. If a piece is within the work space of the manipulator, it is assumed that it can be properly assembled. To avoid collision between different bases, the algorithm intends to maximize the distance between any two bases with a buffer length. This lightens the load of complex collision avoidance constraints on mission planning and control system. Moreover, since the time taken for installation of a piece may vary due to several conditions, this is incorporated into the algorithm as a time delay. This addition is precarious since a large time delay implies a very slow solution whereas a small time delay may cause manipulators to not finish each installation operation on time. The optimization problem can be written as:

$$\min_{\mathbf{N},\,\mathbf{M}} \left(a_1 \cdot \sum_i L_l(i) + a_2 \cdot \sum_i L_r(i) - g\left(\left\|\mathbf{r}_i - \mathbf{r}_j\right\| - 2L\right) \right)$$

where $\mathbf{N} = [\mathbf{N}_1, \mathbf{N}_2, \mathbf{N}_3]$ and $\mathbf{M} = [\mathbf{M}_1, \mathbf{M}_2, \mathbf{M}_3]$ represent the left and right assembly sequence vectors respectively. Here, the symmetry of assembly has been removed. A robot can stay in the same position while other robots assemble and T_{delay_max} denotes the maximum acceptable delay period. $g\left(\left\|\mathbf{r}_i - \mathbf{r}_j\right\| - 2L\right) = \sum_n \min\left(\left\|\mathbf{r}_i(n) - \mathbf{r}_j(n)\right\| - 2L\right), \forall \mathbf{r}_i, \mathbf{r}_j$ is the cost function representing the sum of the minimum relative distances between manipulators at each time step. This optimization problem can be solved using existing algorithms but with low efficiency and high computational cost.

To efficiently solve the optimization problem, a hybrid algorithm, the Continuous Path Generation Algorithm (CPGA) is mapped to the path with work space coverage. For a manipulator located at $\mathbf{r}$, the surrounding pieces (in work space $W(\mathbf{r})$) are recognized by the CPGA and stored from which the rest of the path generation operation is determined. The algorithm stops when all pieces within the working region are installed. It is observed that the mapping is injective; i.e. different CPGAs will generate different paths considering the work space coverage.

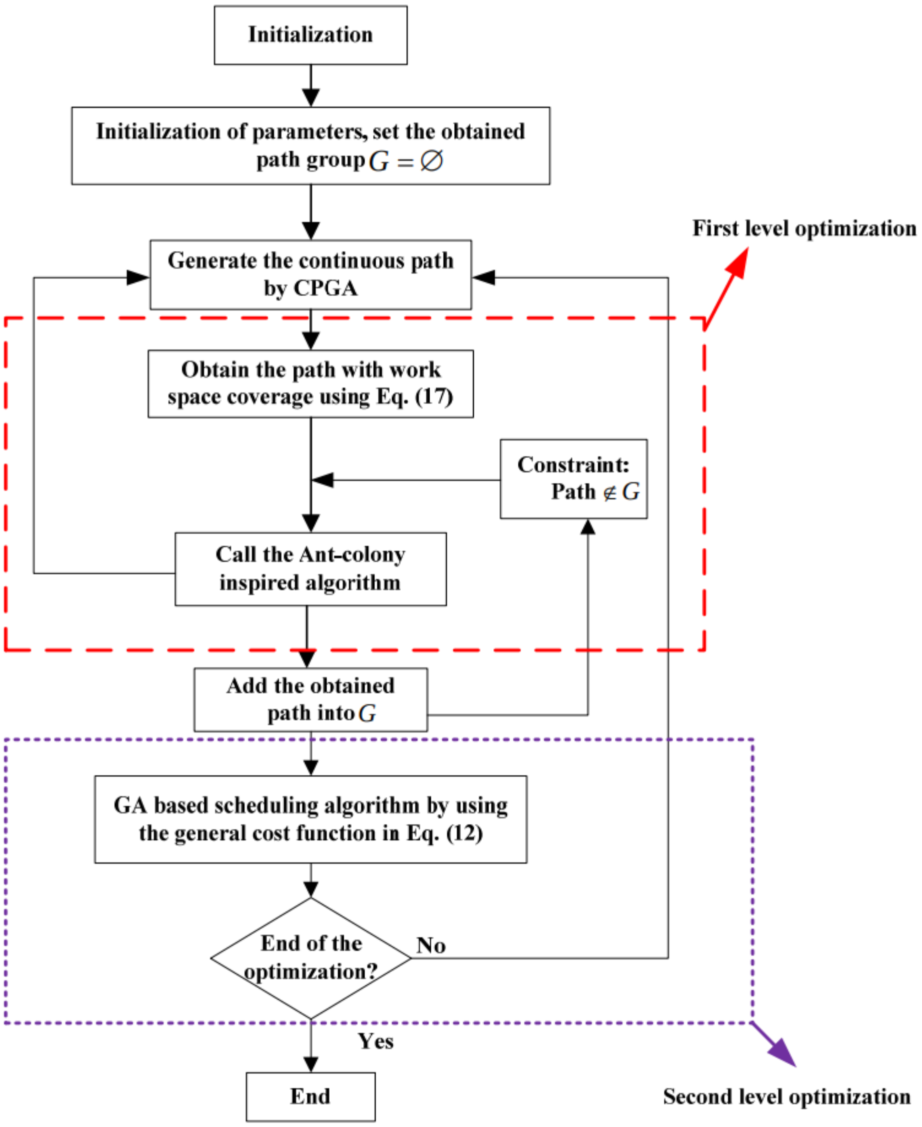

Figure 4.2: Two-level optimization algorithm (She and Li (2020))

Based on the optimization model developed so far, the entire process can be separated into two phases: the first involves path optimization to find the minimum path length using an ant colony-inspired algorithm, and the second is the scheduling of the manipulators considering the delay time and maximizing inter-robotic distance. Given in Fig. 4.2 is a diagram denoting the two-level algorithm adopted for optimization.

4.4 Spacecraft Assembly based on Potential Field

Chen et al. (2017) deal with a particular case of formation control where agents require close proximity and contact using which they assemble to form a larger object. On-orbit assembly has been previously exhibited by the construction of space stations such as Mir and ISS. The motivation of the paper lies in the fact that no previous research has studied on-orbit collision-free assembly of multiple flexible spacecraft using a potential field based control. A form of assembly is developed where agents assemble themselves without utilizing 'assembler robots'.

4.4.1 The Problem

The problem considers multiple spacecrafts (four in the paper) with flexible arms in opposite directions and a hub in the center (hub-beam mechanism). The dynamic equation are given as:

$$\mathbf{M}_i(\mathbf{q}_i)\ddot{\mathbf{q}}_i + \mathbf{C}_i(\mathbf{q}_i, \dot{\mathbf{q}}_i)\dot{\mathbf{q}}_i + \mathbf{g}_i(\mathbf{q}_i) = \tau_i$$

where i represents the agent index, $\mathbf{M}_i$ and $\mathbf{C}_i$ are the mass matrix and the damping matrix respectively, $\mathbf{g}_i(\mathbf{q}_i) = \frac{\partial V}{\partial \mathbf{q}_i}$ is the elastic force vector due to potential energy V, $\mathbf{q}_i = [\mathbf{X}_i\ \mathbf{p}_i]^T = [X_o\ Y_o\ \theta\ p_{A1}\ p_{B1}]^T$ is the generalized coordinate vector, and $\tau_i = [\tau_{i1}^T\ \mathbf{0}^T] = [F_x\ F_y\ T_0\ 0\ 0]^T$ is the generalized external force vector, composed of the forces acting on the spacecraft's center and the moment acting on the spacecraft. The only observable states are $\mathbf{X}_i$ and $\dot{\mathbf{X}}_i$, and since only the rigid hub is controllable, the flexible spacecraft is an underactuated system.

Communication between the agents is done as per an undirected ring graph, whereby an agent can communicate with its neighboring two agents. Also, given arbitrary position, orientation and deformation of appendages, the agents are expected to form a pre-assembly configuration and then move into an assembly configuration as shown in Fig. 4.3. The central region in between the flexible spacecrafts in the pre-assembly configuration is further considered as a virtual leader which is followed by each agent.

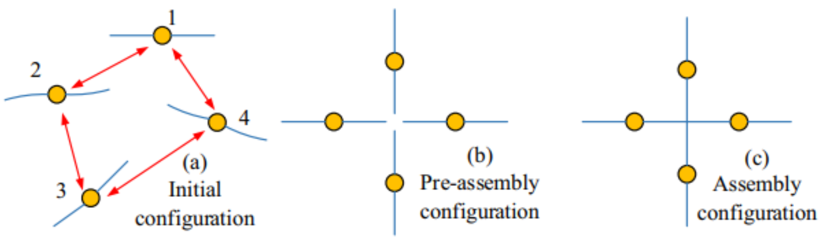

Figure 4.3: Configuration Transformations (Chen et al. (2017))

4.4.2 The Solution

An artificial potential field can be introduced that needs to be minimized to achieve the final configuration. Each spacecraft is considered to lie inside an ellipse whose center coincides with the center of the rigid hub, and whose major axis and minor axis lengths are $R+L$ and R respectively. The potential field can be divided into the following parts:

- The virtual leader is considered to be at the point of average coordinates of the agents from their initial configuration with a safety radius of δ. For each agent to move closer to the virtual agent, a potential field is defined as: $V_1 = \sum_{i=1}^{4} \beta_1 d_{i0}^2$, where d_{i0} is the distance between the ellipse of agent i and the virtual leader circle
- In order to enforce an orientation angle difference of $\frac{\pi}{2}$ between each neighboring agent, a potential field is provided as: $V_2 = \beta_2 \sum_{i=1}^{3} cos^2(\theta_{i+1} - \theta_i)$
- Each rigid hub is expected to be as far away as possible from the virtual hub while satisfying $V_{i1} = 0$ in order to create a configuration as shown in Fig. 4.3. Hence, the centers of the virtual leader and the rigid hub should be at a distance of $R+L+\delta$, and a potential field is defined as: $V_3 = \sum_{i=1}^{4} \beta_3 \left[\sqrt{(X_{0i} - X_L)^2 + (Y_{0i} - Y_L^2)} - (R+L+\delta) \right]^2$

The total potential energy of the assembly mission is given as $V_A = V_1 + V_2 + V_3$ where $V_1 \geq 0$, $V_2 \geq 0$, $V_3 \geq 0$ and hence $V_A \geq 0$ are always true. However, in order to avoid local minima, V_1 is rewritten as $V_1^* = \sum_{i=1}^{4} \beta_1 \left[(X_{0i} - X_L) sin\theta_i - (Y_{0i} - Y_L) cos\theta_i \right]^2$, giving $V_A^* = V_1^* + V_2 + V_3$. Furthermore, to avoid inter-spacecraft collision, a fourth potential is develop as $V_4 = \sum_{i=1}^{4} \sum_{j \in N_i} V_{ij} = \sum_{i=1}^{4} \sum_{j \in N_i} \beta_4 \left[coth\left(\frac{d_{ij} - \gamma}{K_{ij}} \right) - 1 \right]$

4.5 Spacecraft Assembly based on Disturbance Observer

Chen and Wen (2018) deal with the assembly of large space structures where each module can control its own motion to gain the desired states. Previous research has conducted this study for rigid spacecrafts. Here, the problem is proposed for flexible spacecrafts.

4.5.1 The Problem

Assembly of rigid spacecraft has been studied in previous research. However, this is not capable of considering the effect of appendages such as solar panels, antennas and manipulators. A control law can be designed with a disturbance observer for the assembly of multiple flexible spacecraft into a large structure. Two topologies are used for the system: $\mathscr{G}_1$ for basic information communication and $\mathscr{G}_2$ for collision avoidance. The former utilizes a graph such that a given node receives information of nodes with adjacent numbers, and hence is a constant graph. On the other hand, the latter utilizes a graph such that an edge is formed between two nodes if the distance between them is less than a constant value α, and hence is time-variant.
The spacecrafts form a pre-assembly configuration following which they move closer to assemble. The latter step is very easy and only an assembly controller is required. Pre-assembly incorporates a compound controller consisting of the assembly controller and a collision avoidance controller. The spacecraft is controlled by manipulating the rigid hub which is the only observable part of each spacecraft. Each spacecraft consists of a rigid hub and two flexible appendages (A, B), and is treated as an Euler-Bernoulli beam (Refer to Glossary). The generalized coordinate vector for spacecraft i can hence be written as $\mathbf{q}_i = [X_{0i}\ Y_{0i}\ \theta_i\ p_{A1i}\ p_{A2i}\ p_{A3i}\ p_{B1i}\ p_{B2i}\ p_{B3i}]$, where $\mathbf{x}_i = (X_{0i}\ Y_{0i}\ \theta_i)$ gives the coordinates of the rigid hub of spacecraft i, and $\mathbf{p}_i = [p_{Aki}]$ and p_{jki} gives the k-th modal component of appendage j of spacecraft i. This gives the dynamic equation in matrix form as:

$$\mathbf{M}_i(\mathbf{q}_i)\ddot{\mathbf{q}}_i + \mathbf{C}_i(\mathbf{q}_i,\dot{\mathbf{q}}_i)\dot{\mathbf{q}}_i + \mathbf{C}_{di}\dot{\mathbf{q}}_i + \mathbf{K}_i(\mathbf{q}_i)\mathbf{q}_i = \mathbf{G}_i\tau_{ix}$$

where $\mathbf{M}_i$ is the mass matrix, $\mathbf{C}_i\dot{\mathbf{q}}_i$ is the summation of the centrifugal and the Coriolis torque/force, $\mathbf{C}_{di}\dot{\mathbf{q}}_i$ is the structural damping force, $\mathbf{K}_i$ is the stiffness matrix, $\mathbf{G}_i = [\mathbf{I}_3\ 0_{3\times 6}]^T$, and τ_i is the control input vector.

4.5.2 The Solution

The paper presents a disturbance observer which approximates to the value of the disturbance forces. Since the rigid hub is the only part of the spacecraft which can be manipulated, the vibrations caused on the appendages are considered as disturbances. The disturbance observer incorporates the state vector ($\mathbf{z}_i$) and a non-linear function ($\mathbf{f}(\dot{\mathbf{x}}_i)$) of the derivative of the coordinates of the rigid hub. Provided that $g(\dot{\mathbf{x}}_i) = \frac{\partial \mathbf{f}(\dot{\mathbf{x}}_i)}{\partial \dot{\mathbf{x}}_i} = \mathrm{diag}([\lambda_1(\dot{\mathbf{x}}_{i1})\ \lambda_2(\dot{\mathbf{x}}_{i2})\ \lambda_3(\dot{\mathbf{x}}_{i3})])$ where λ_i is a positive function of x_i for all i, the disturbance estimation errors gradually converge to zero. The paper defines an auxiliary variable $\bar{\mathbf{x}} = \mathbf{x} - \Delta$, where Δ is a constant offset vector defined by the final configuration of interest. The assembly controller aims to equate this variable for every agent; i.e. $\bar{\mathbf{x}}_1 = \bar{\mathbf{x}}_2 = \ldots = \bar{\mathbf{x}}_N$. A control law without collision avoidance can be developed for this purpose and the fleet of flexible spacecraft can be driven to the required pre-assembly configuration with a gradual suppression of the appendage vibrations using this control law. When the agents are very close to each other, collision avoidance is achieved by introducing a repulsive potential field defined as: $V_{ca} = \sum_{i=1}^{N} \sum_{j \in N_{2i}} V_{ca,ij}$ where N_{2i} represents the set of neighbors of node i in the collision avoidance graph $\mathscr{G}_2$ and

$$V_{ca,ij} = \begin{cases} (D_{ij} - \alpha)^2, \text{ if } D_{ij} \leq \alpha, \\ 0, \text{ otherwise} \end{cases}$$

where D_{ij} is the radial Euclidean distance between the ellipses formed by agents i and j. The collision avoidance force is given as $F_{ca} = -\nabla_x V_{ca}$ which is added to the control input force τ_x. This force is included in the control law in order to bring the agents to the pre-assembly configuration. However, it is not used to achieve the assembly configuration since an input of very small distances to the collision avoidance potential may cause adverse results.

Chapter 5

Recent Developments in Spacecraft Attitude Control

5.1 A Consideration of Thrust Uncertainty

Golpashin et al. (2020) deal with modeling and mitigating disturbances caused by a spacecraft itself, specifically thrust-induced disturbances of continuous low-thrust spacecraft attitude maneuvers. These disturbances are modeled as a multiplicative Gaussian white noise process along with the existing noise in thrust, and a stochastic optimal controller is designed to obtain the behavior based on the best-known information on the severity of the disturbance.

Spacecraft attitude dynamics can be modeled as stochastic differential equations (Refer to Glossary) with the control law based on the multiplicative nature of increasing the magnitude of thrust on the propagated thrust uncertainty. All initial conditions and state variables are known ahead of time and a Hamilton-Jacobi-Bellman (HJB) equation is formulated to give a solution approximated by a power series. The solution is local in nature and suboptimal away from the origin, but in the operational space, the control is approximately optimal.

There are three methods adopted in previous research to formulate attitude dynamics. The first uses a cascade structure, the second uses a Hamiltonian formulation to represent dynamic and kinematic equations as a second-order differential equation, and the third adjoins the kinematic and dynamic equations by extending the state vector of the kinematic parameters and the body rotational axes. Here, the third approach is adopted to approximate the HJB equation; hence, the closed-loop nonlinear equation is stable in the neighborhood of the origin.

5.1.1 The Problem

The system is represented using the dynamic equations $I\dot{\omega} = S(\omega)I\omega$ where $S(\omega)$ is the cross product matrix of ω, $I \in \mathbb{R}^{3\times3}$ is the principal moment of the inertia matrix, $\omega \in \mathbb{R}^{3\times1}$ is the angular velocity vector about the body principal axes, and M is the total applied torque vector. The Tsiotras-Longuski parameterization (Refer to Glossary) is used to describe orientation since it involves only three parameters for a system of three degrees of freedom. Also it contributes to a linear component in the system, hence permitting the system to be linearized at the defined state's origin. Moreover, the structure of the involved differential equations allows a 'degree-by-degree approximation' of the system to the origin, starting from linear control. Finally, in contrast to Euler angle parameterization, the singularity is at a more desired position.
A single thruster fired with a force $F = [\cos(\alpha)\sin(\beta)\ \sin(\alpha)\sin(\beta)\ \cos(\beta)]^T \acute{\boldsymbol{F}}$ oriented with azimuth angle α and elevation angle β and located at $r = r_1e_1 + r_2e_2 + r_3e_3$ from the center of gravity of the spacecraft gives a thrust to the spacecraft as $\tau = r \times F = b\acute{\boldsymbol{F}}$. The spacecraft can have multiple bidirectional thruster pairs generically indexed as i, and the thrusters in a pair are symmetric to each other ($r_{i1} = -r_{i2} = r_i$) though the forces F_{i1} and F_{i2} may be different. The total thrust due to such a pair is: $\tau_i = r_{i1} \times F_{i1} + r_{i2} \times F_{i2} = r_i \times \frac{||F_{i1}||+||F_{i2}||}{||F_{i1}||} \cdot F_{i1} = r_{i1} \times F_i$, where F_i gives the equivalent net force resulting in the generalized torque due to the ith thruster pair. The torques of m such pairs can be accumulated to give the total exerted torque $\boldsymbol{\tau} = bU_{NF}(t)$, where $U_{NF}(t)$ is the total noise-free control vector and each column b_i (assume time-invariant) of $b : \mathbb{R}^3 \to \mathbb{R}^m$ represents the axes about which $||b_i||U_{NF,i}(t)$ is applied. Substituting the generalized moment as $bU_{NF}(t)$, the system dynamic equations can be reformulated as:

$$I\dot{\omega} = S(\omega)I\omega + bU_{NF}(t)$$

The thrust uncertainty of the ith thruster can be given as an independent Gaussian white noise process η_{ti} from which the uncertainty due to the thruster pair can be modeled as a Gaussian white noise process $\xi_t = \eta_{t1} + \eta_{t2}$. The noisy control input is $U_i(t) = U_{NF,i}(t)(1 + \xi_{ti})$ and the total control input $U(t)$ is the sum of all $U_i(t)$. Unlike additive noise, the multiplicative uncertainty structure lets the magnitude of noise generated by the to be dependent on the magnitude of the control input itself. On solving the dynamics equation with the control input model and replacing the noise component with the diffusion coefficient $\sigma(.)$ and the m-dimensional standard Brownian motion W_t (Refer to Glossary) on the probability space $(\Omega, \mathscr{F}, \mathbb{P})$, we get:

$$\omega_t = \omega_0 + \int_{t_0}^{t} [I^{-1}S(\omega_s)I\omega_s + I^{-1}bu(s)]ds + \int_{t_0}^{t} \sigma(u(s))dW_t$$

The state vector is defined as $x = [\omega_1\ \omega_2\ \omega_3\ w_1\ w_2\ z]^T$ and, on differentiating, gives the equation of the complete system with suitable coefficients as:

$$dx = [Ax + f^{(2)}(x) + f^{(3)}(x) + Bu(t)]dt + \sigma(u(t))dW_t$$

where the superscripts in parenthesis represent the order of the terms in the state. The diagonal nature of the control input matrix allows each entry of the Wiener process to be solely associated with the corresponding input $u_i(t)$.

5.1.2 The Solution

The control algorithm involves the minimization of a cost function $\mathscr{J}(u) = \mathbb{E}_{x_0,t_0}\left[\int_{t_0}^{\infty} r(x,u)dt\right]$, where we have an infinite time horizon, $t_0 \geq 0$ is the initial time and x_0 the previously determined initial state. The value function (minimum cost) $V(x)$ is the solution to the HJB equation associated with the stochastic differential equation that describes the complete system:

$$min_u[\mathscr{L}^u V(x) + r(x,u)] = 0$$

where $\mathscr{L}^u V(x)$ is a function of the single and double partial derivatives of $V(x)$. Given $V(x)$ and corresponding $u(x)$, the control $u = u(x)$ is optimal and will minimize the functional in infinite time if $V(x)$ satisfies the asymptotic stability conditions of Lyapunov's second method for SDEs, $V(x)$ satisfies $\mathscr{L}^u V(x) = -r(x,u)$ given the closed-loop system, and a particular Hamiltonian [1] is strictly convex in κ and attains its minimum when $\kappa = u$. Given these conditions, we aim at finding approximations for the solution to the HJB equation as a truncated series.

Supposing $u(k)$ and $V(k)$ to be the optimal solutions, they are approximated as power series substituted in the HJB equation to give the Hamiltonian, which is further differentiated to give a control equation. A particular matrix K can be developed such that the linear control Kx asymptotically stabilizes the linear dynamics of the system in probability, and is optimal with respect to the quadratic Hamiltonian based on the satisfaction of two conditions. Considering two specific linear operators $L_1 = ((A+BK)x)^T \frac{\partial}{\partial x}$ and $L_2 = \frac{1}{2}\varepsilon^2(BKx)(BKx)^T H$, non-linear stochastic control $k^{(m)}(x)$ for $m > 2$ can also be developed, provided the asymptotic stability of the linear deterministic part of dynamics and that the minimum eigenvalue of L_1 acting on $V^{(m)}(x)$ is greater than the maximum eigenvalue of L_2.

The general SDE $dx_t = f(t,x_t)dt + \sigma(t,x_t)dW_t, t \geq 0$ representing the system linear dynamics for any drift function $f(t,x_t) \in \mathbb{R}^n$ shows asymptotic stability in probability, provided a particular time-dependent 'counterpart' of the infinitesimal generator $\mathscr{L}$ satisfies $\mathscr{L}V(t,x) < -CV(t,x)$; i.e. $\mathscr{L}V(t,x)$ is negative definite, for an arbitrary constant $C > 0$ and positive definite function $V(t,x) : [t_0,\infty) \to \mathscr{X} = \{x : |x| < h, h > 0\}$, that is twice differentiable in x and differentiable in t. Up to sextic non-linear control can be solved with each order of control containing unknowns from the Hamiltonians of the next order; in order to solve the system for six terms, the value function needs to be known until $n = 7$.

5.2 Attitude Consensus based on Distributed Observers

Distributed attitude consensus of multiple cooperative spacecrafts can be classified as two types: leaderless consensus where spacecrafts reach an a priori unknown state, and leader-following consensus where each follower tracks a prescribed trajectory provided by a real or virtual leader. Gui and de Ruiter (2018) focuses on the leader-following method in terms of quaternion parameterization and develops a novel non-linear distributed observer while assuming the communication graph between followers to be undirected and complete such that global finite-time

[1] $\mathscr{H}(x,\kappa,V(x)) = f(x,\kappa)^T \frac{\partial V(x)}{\partial x} + \frac{1}{2}\text{trace}\left(a(\kappa)\frac{\partial^2 V(x)}{\partial x^2}\right) + r(x,\kappa)$

convergence is assured even when only a single follower is connected to the leader.

5.2.1 The Problem

The equations of motion of the ith agent can be written as:

$$\dot{Q}_i = \frac{1}{2} Q_i \circ \omega_i = \frac{1}{2} E(q_i)\omega_i = \frac{1}{2} \begin{bmatrix} -q_i^T \\ q_i^\times + \eta_i I_3 \end{bmatrix}$$

$$J_i \dot{\omega}_i = -\omega_i \times J_i \omega_i + u_i$$

where $\omega_i \in \mathbb{R}^3$ and $J_i = J_i^T$ are the angular velocity and inertia tensor of the agent expressed in the body frame $\mathscr{F}_i$, and the leader is indexed as 0. If all followers are connected to the leader, it is sufficient to globally stabilize $(Q_{i0}, \omega_{i0}) = (\pm\mathbf{1}, 0), i \in \mathbb{I}_n$. Information flow, being bidirectional, is given by a weighted undirected graph $G = (\mathscr{V}, \mathscr{E})$, and the leader-following graph as $\bar{\mathscr{G}} = (\bar{\mathscr{V}}, \bar{\mathscr{E}})$ where $\bar{\mathscr{V}} = \{0\} \cup \bar{\mathscr{V}}$ and $\bar{\mathscr{E}} \subseteq \bar{\mathscr{V}} \times \bar{\mathscr{V}}$. The following are assumed:

- All spacecraft share the same inertial frame $\mathscr{F}_I$.
- Communication among followers is constant and bidirectional.
- $\bar{\mathscr{G}}$ has a spanning tree rooted at node 0 (a path exists from the leader to any follower).
- The leader's angular velocity $\omega_0(t)$ and its first two derivatives are continuous in time.
- There exists constants $\gamma_i, i \in \mathbb{I}_3$ s.t. $||\omega_0(t)||_\infty \leq \gamma_1$, $||\dot{\omega}_0(t)||_\infty \leq \gamma_2$, and $||\ddot{\omega}_0(t)||_\infty \leq \gamma_2$.

5.2.2 The Solution

5.2.2.1 Distributed Finite-Time Observer Design

A non-linear distributed observer can be developed to obtain the leader's trajectory $(Q_0, \omega_0, \dot{\omega}_0)$ for each agent in finite time when only a subset of the followers can access the leader's attitude and angular velocity relative to the inertial space. Assuming that the estimate of the leader's trajectory, $(P_i, v_i, z_i) \in \mathbb{R}^4 \times \mathbb{R}^3 \times \mathbb{R}^3$ is equal to the trajectory itself, the observer is designed as:

$$
\begin{aligned}
\dot{P}_i &= \frac{1}{2} P_i \circ v_i - \lambda_1 \operatorname{sgn}^{\beta_1}\left(\sum_{j=0}^{n} a_{ij}(P_i - P_j)\right) \\
\dot{v}_i &= z_i - \lambda_2 \operatorname{sgn}^{\beta_2}\left(\sum_{j=0}^{n} a_{ij}(v_i - v_j)\right) \\
\dot{z}_i &= -\lambda_3 \operatorname{sgn}\left(a_{i0}(z_i - w_i) + \sum_{j=0}^{n} a_{ij}(z_i - z_j)\right)
\end{aligned}
$$

where $(P_i(0), v_i(0), z_i(0)) \in \mathbb{R}^4 \times \mathbb{R}^3 \times \mathbb{R}^3, i \in \mathbb{I}_n, \lambda_1, \lambda_2, 0 < \beta_1, \beta_2 < 1, \lambda_3 > \gamma_3$. The leader's angular acceleration $\dot{\omega}_0$ is not available to followers and is calculated using a second-order sliding mode differentiator. The equations of the estimation errors can be written based on the equations of the observer. Given the assumptions in 5.2.1, the state estimates are all uniformly bounded and the estimate is equal to the leader's trajectory beyond an instance T_p.

Unlike previous research, it is only required for the leader's trajectory to be bounded and continuous, and finite-time convergence ensures high accuracy. Higher-order sliding modes can produce better accuracy and less sensitivity to input noise during digital implementation. Moreover, this distributed observer can be readily extended to the double integrator systems and Euler-Lagrange systems. However, $P_i(t)$ may not be a unit quaternion in $0 \leq t \leq T_p$. Moreover, the stability of the system does not ensure global stability on $SO(3)$ and unwinding can occur. This can be reduced by reducing T_p by increasing $\lambda_i, i = 1,2,3$.

5.2.2.2 Consensus Law Design

Since the attitude estimate need not be a unit quaternion, finite-time escape of the closed-loop trajectory should be prevented. This is done by incorporating global finite-time attitude controllers with full-state measurements and attitude-only measurements into the observer.

Full-State Measurements : A hybrid controller can be developed for followers (say i) that are directly connected to the leader such that the global finite-time stability of the equilibrium set $\mathscr{E}_i = \{\boldsymbol{x}_{fi} \in \mathscr{M}_i \colon Q_{i0} = h_i \mathbf{1}, \omega_{i0} = 0\}$ is ensured, where $h_i \in \mathbb{H} = \{-1, 1\}$, $\boldsymbol{x}_{fi} = (Q_{i0}, \omega_{i0}, h_i), i \in \mathbb{I}_n$ and $\mathscr{M}_i = \mathbb{S}^3 \times \mathbb{R}^3 \times \mathbb{H}$. The control law involves two control modes depending on whether $h_i \eta_{i0}$ or δ (between 0 and 1) is greater. This controller cannot be applied for a follower that does not have access to the leader, due to which estimates equal to the actual values for $t \geq T_p$

are developed. It is possible to have unbounded control torques for $0 \leq t \leq T_p$. To keep them bounded, a new function is defined for the control input, such that only finite energy is injected into the closed-loop system, hence removing the disadvantage of finite escape time. Such a leader-following spacecraft system with the specified hybrid control law along with the distributed observer ensures the uniform boundedness of $(Q_{i0}(t), \omega_{i0}(t))$ and globally stabilizes $(Q_{i0}(t), \omega_{i0}(t))$ to $(h_i\mathbf{1}, 0) \in \mathbb{S}^3 \times \mathbb{R}^3, i \in \mathbb{I}_n$ in finite time. The proposed consensus scheme also removes the requirement of communicating the binary logic variable h_i between neighboring agents, leading to a simpler switching logic.

In a real-life scenario, switching based on the logic variable h_i will be a continuous approximation for the actuator. If the actuator responds 'fast enough', the effect of this hysteretic switching can be well-approximated. It has been previously shown that the maximum number of switching is proportional to the initial kinetic energy. Hence, the number and speed of switching can be reduced by initializing with small initial angular velocity errors.

Attitude-only Measurements : Follower i can track its attitude Q_i but not its angular velocity ω_i. Moreover, the transient nature of Q_{i0} is absent for $t \geq T_p$. A controller can be developed similar to the previous case but with h_i and $\tilde{h}_i$ (switching variable associated with $\tilde{Q}_{i0}$). A leader-following spacecraft system with this hybrid control law combined with the distributed observer ensures the uniform boundedness of $(\tilde{Q}_{i0}(t), Q_{i0}(t), \omega_{i0}(t))$ and globally stabilizes $(\tilde{Q}_{i0}(t), Q_{i0}(t), \omega_{i0}(t))$ to $(\tilde{h}_i\mathbf{1}, h_i\mathbf{1}, 0) \in \mathbb{S}^3 \times \mathbb{S}^3 \times \mathbb{R}^3, i \in \mathbb{I}_n$, in finite time, where $\tilde{Q}_{i0} = \bar{Q}_{i0}^* \circ \hat{Q}_{i0}$ is the quaternion error between $\hat{Q}_{i0}$, the estimate for Q_{i0}, and $\bar{Q}_{i0}^*$, an alternative that substitutes for the necessary damping achieved by the direct use of angular velocity. In this problem, fixed communication topology and zero state measurement time delays are assumed. Moreover, although previous research has given solutions for leaderless attitude consensus with time-varying topologies, angular velocities were treated as inputs. Dealing with such topologies for distributed attitude observers is an open research topic.

5.3 Attitude Synchronization and Tracking Control over a Communication Network with a Switching Topology

Attitude synchronization is the problem of bringing multiple spacecraft attitudes into an agreement. On the other hand, attitude tracking involves multiple spacecraft tracking a common reference as a virtual leader in a cooperative way, where this reference is only available to a portion of spacecraft. In most cases, the proposed control algorithms are applicable only using fixed network topology; i.e., each initial communication link between distinct spacecraft is maintained all the time. This may not be possible in reality due to practical issues such as environment disturbance, communication range and perturbation; hence, it is required to develop coordinated attitude control algorithms using switching topologies (Refer to Glossary).
Previous research involving switching topologies requires switching between (quasi-strongly) connected subgraphs; i.e. each spacecraft has a connection link with at least one of its neighbors all the time, which is a restrictive requirement. Liu et al. (2020) considers a switching topology with the milder requirements of uniform joint connectivity (for synchronization) or uniform joint quasi-strong connectivity (for tracking), and adaptive schemes designed to deal with the unavailability of inertial parameters, hence allowing spacecraft to lose contact with others for some time. The algorithms are developed by simultaneously exploring the attitude kinematics and dynamics without exact knowledge of inertial parameters, and a distributed observer is proposed since leader reference information is only partially available.

5.3.1 The Problem

A group of n spacecraft is considered whose orientation in the body-fixed frame $\mathscr{B}_i$ with respect to an inertial frame $\mathscr{I}$ is represented by modified Rodrigues parameters (MRPs, Refer to Glossary) σ_i, and rotation matrix R_i represents the rotation from $\mathscr{B}_i$ to $\mathscr{I}$. MRPs are used since they exhibit singularities at $\pm 2\pi$, which can be avoided by switching to the other MRP representation (σ or $-\frac{\sigma}{\sigma^T\sigma}$). The kinematics and dynamics of the attitude system of each spacecraft are given as:

$$\dot{\sigma}_i = G(\sigma_i)\omega_i$$
$$J_i\dot{\omega}_i = -\omega_i^{\times} J_i\omega_i + \tau_i$$

where ω_i is the angular velocity in $\mathscr{B}_i$, J_i is the inertial matrix with respect to $\mathscr{B}_i$, τ_i is the control torque in $\mathscr{B}_i$, and $G(\sigma_i) = \frac{1}{2}\left[\frac{1-\sigma_i^T\sigma_i}{2}I_3 + \sigma_i^{\times} + \sigma_i\sigma_i^T\right]$. The dynamics of a leader spacecraft indexed 0 is also defined in a similar manner, and the reference angular velocity ω_0 can be a finite combination of any step function and sinusoidal function. Two control objectives need to be solved while imposing constraints on the system:

- **Coordinated attitude synchronization**: Develop a distributed control algorithm such that all the spacecraft attitudes reach a synchronization over a switching network, i.e.,

$$\lim_{t\to\infty}(\sigma_i(t) - \sigma_j(t)) = 0, \lim_{t\to\infty}\omega_i(t) = 0, \forall i, j \in \mathscr{V}$$

- **Coordinated attitude tracking**: Develop a distributed control algorithm such that all the spacecraft attitudes track the reference attitudes σ_0 and the angular velocity ω_0 simultaneously over a switching network, i.e.,

$$\lim_{t\to\infty}(\sigma_0(t)^{-1}\circ\sigma_i(t)) = 0, \lim_{t\to\infty}(\omega_i(t) - \omega_0(t)) = 0, \forall i \in \mathscr{V}$$

5.3.2 The Solution

5.3.2.1 Coordinated Attitude Synchronization

The switching graph is assumed as undirected and uniformly jointly connected, and given the vectors $a = [a_1, a_2, a_3]^T$ and $\theta_i = [J_{i,11}, J_{i,22}, J_{i,33}, J_{i,12}, J_{i,13}, J_{i,23}]^T$, a linearization operation $M(a)$ is introduced such that $J_i a = M(a)\theta_i$. A coordinated adaptive control algorithm is proposed that gives τ_i and $\hat{\theta}_i$ (estimate of θ_i) in terms of ω_i, σ_i, and the adjacency matrix $A_{\zeta(t)}$. The absolute attitude information is delivered via the communication network. Here, each spacecraft does not have exact knowledge of its inertial parameter J_i due to which θ_i is unknown and hence estimated, and this estimate is fed into the dynamics equation of the spacecraft. The paper develops an algorithm that achieves attitude synchronization provided the satisfaction of a particular criterion on the control parameters of the algorithm.

5.3.2.2 Coordinated Attitude Tracking

The leader-follower graph is assumed to be uniformly jointly quasi-strongly connected and the follower graph is undirected. The tracking problem can be solved in two steps:

Distributed Observer Design : The estimates of the MRPs and the velocity of the leader are calculated at each agent by a distributed observer that depends on the previous estimate and the error in estimation. The estimation error system derived from the observer is shown to be asymptotically stable provided constraints on the maximum value of estimation error at $t = 0$. This is proven in four steps wherein a particular Lyapunov function dependent on the velocity error is shown to be constrained in piecewise time intervals and hence goes to 0 as $t \to \infty$ due to which velocity error and, therefore, MRP error goes to 0 as $t \to \infty$.

Tracking Control Development : Given the dynamics of the attitude error $\sigma_i^e = \dot{\sigma}_i^{-1} \circ \sigma_i$, the tracking control $\tau_i, \forall i \in \mathscr{V}$ is proposed along with an estimate for θ_i. For the given spacecraft system conditions, the proposed tracking control guarantees that the attitude tracking objective is achieved. This is proven using a suitable Lyapunov function that gives $\lim_{t\to\infty} \omega_i^e(t) = 0$ using Barbalat's Lemma (Refer to Glossary), further giving $\lim_{t\to\infty} \sigma_i^e(t) = 0$ and $\lim_{t\to\infty} R(\sigma_i^e) = I_3$, from which we get $\lim_{t\to\infty}(\omega_i(t) - \hat{\omega}_i(t)) = 0, \forall i \in \mathscr{V}$.

Chapter 6

Results and Discussions

6.1 Introduction

This chapter discusses the results obtained from simulations performed by the authors of relevant publications. The corresponding inferences are also explained to some extent. Chapter 3 has been excluded since the research works discussed therein were mostly written as surveys on previous existing work. Hence, this chapter focuses on recent developments in the fields of spacecraft formation control and attitude control.

6.2 Decentralized Formation Flying

Sakurama et al. (2019) consider six agents in $\mathbb{R}^2$ configured as a graph with four maximal cliques of order 3. The desired formation is achieved at $t = 40$ with some rotation and translation. Each agent at $x_i(t)$ is matched to a desired position $\hat{x}_{*ik}(t) = R_{C_k}(x_{*k}) + \tau_{C_k}(t)$ for each clique C_k. These matched desired positions, though initially separated, gather gradually to form the desired formation. Collision avoidance can also be incorporated as a repulsive potential force in $v(X)$. Secondly, seven agents in $\mathbb{R}^3$ are configured with four maximal cliques of order 4. The desired formation is again achieved at $t = 40$ without reflections owing to distributed pattern matching. This is not the case with the existing method that uses the distance-based controller, where final agent positions may be different from desired positions due to reflections.

To develop a graph condition to achieve an indicator to $\mathscr{T}_{X_*}$, the concept of a *framework* is defined: a pair (G,X) for graph G and matrix $X \in \mathbb{R}^{d\times n}$. The framework (G,X_*) is *clique-rigid* if, for each matrix $X = [x_1\ x_2\ \ldots\ x_n]$,

$$[x_j]_{j\in\mathscr{C}} \in \mathscr{P}_{\mathscr{C}}(\mathscr{T}_{X_*})\ \forall\mathscr{C} \in \text{M-clq}(G) \implies X \in \mathscr{T}_{X_*}$$

The paper states a number of theorems based on this:

- (G,X_*) is clique-rigid if it is the only framework that can be constructed from the set of the frameworks $(G|_{\mathscr{C}}, [x_{*j}]_{j\in\mathscr{C}})$ induced by the maximal cliques $\mathscr{C} \in \text{M-clq}(G)$.
- There exists an indicator v to target set $\mathscr{T}_{X_*}$ if and only if (G,X_*) is clique-rigid.
- Framework (G,X_*) is clique rigid if (but not only if) (G,X_*) is globally rigid and there exists a clique $\mathscr{C}$ satisfying $|\mathscr{C}| \geq d+1,\ [x_{*j}]_{j\in\mathscr{C}} \in \mathscr{M}_{d|\mathscr{C}|}$
- If framework (G,X_*) is clique rigid, (G,X_*) is rigid.

Clique rigidity is stronger than rigidity, and given a clique that satisfies the condition in the third theorem, clique rigidity is weaker than global rigidity. Furthermore, the zero set $\mathscr{Z}(\frac{\partial v}{\partial X})$ is the globally attractive equilibrium set and $v^{-1}(0)$ is a locally attractive equilibrium set of the system $\dot{x}_i(t) = R_i u_i(t)$ with the gradient-based control input as given earlier. Also, if framework (G,X^*) is clique rigid, $\mathscr{T}_{X_*}$ is a locally attractive equilibrium set of this system with the same control input, and if G is complete, $\mathscr{T}_{X_*}$ is the globally attractive equilibrium set.

Ren and Beard (2004) present simulation results for nine spacecrafts (a mothership and eight other ships) developing a circular formation following which they rotate 45° about the inertial z-axis. To test the robustness of the system, the local copies of the coordination vector are instantiated at different time instances, and varying delays of communication and sample times are considered. The simulation is considered for three cases: one without formation feedback and no actuator saturation, one without formation feedback but with actuator saturation, and one with formation feedback amid actuator saturation (the case without actuator saturation but with formation feedback should give similar results as the first case). The average coordination error, $\frac{1}{N}\sum_{i=0}^{N}||\xi_i - \frac{1}{N}\sum_{i=0}^{N}\xi_i||$, is observed to be identical with or without actuator saturation since that does not affect the dynamics of the virtual structure. However, this is larger in the third case since formation feedback can add dissimilarities between different instantiations. The absolute tracking errors for position and attitude are compared for the three cases. Including formation feedback to actuator saturation decreases the error, making it similar to the first case, though at the cost of system convergence time. Similar observations are seen for the relative position and attitude error even with the latter being smaller for case 3 than for case 1. The control forces and torques are also analyzed showing the saturation of τ_z in case 2 which is mitigated using formation feedback.

She and Li (2020) conduct two tests, one for each level of the algorithm (mission planning and mission scheduling). The first one compares results when MATLAB Genetic Algorithm solvers are run on the mission planning problem against the proposed algorithm for a certain set of system parameters. This is done as three parts:

- Considering the symmetric path assembly criterion, the hybrid algorithm shows slight improvement over the genetic algorithm, possibly from the latter reaching a local minima due to complexity.
- Considering the inter-robotic distance criterion, the improvement is not significantly large.
- The first condition is removed to consider asymmetric path assembly. Since many more solutions are possible in this case, the relative inter-robotic distance is further increased.

The second test checks the effectiveness of mission scheduling. The improvement in relative distances is very small without considering delays. Delays are added for the manipulators to wait until the relative distance is larger than a minimum threshold. Meanwhile, an adaptive law decreases this threshold if all robots are blocked. These improvements reduces risks of collision and simplifies the entire process. However, they increase the total assembly period, and due to asymmetry, some regions are completed even before others finish 50% of their work.

Chen et al. (2017) perform simulations for the multi-agent system using the proposed model. There are two cases included in the paper. The first case gives a situation where the agents are scattered on a plane with some close to the virtual agent whereas others being farther: $\mathbf{q}_{10} = [0\ 20\ 0\ 0\ 0]^T$, $\mathbf{q}_{20} = [-20\ 10\ 0\ 0\ 0]^T$, $\mathbf{q}_{30} = [-20\ \ -20\ 0\ 0\ 0]^T$, $\mathbf{q}_{40} = [20\ 10\ 0\ 0\ 0]^T$. In the second case, all agents are placed on a line such that they have to actively change their orientations and move to the virtual leader: $\mathbf{q}_{10} = [0\ 30\ 0\ 0\ 0]^T$, $\mathbf{q}_{20} = [0\ 20\ 0\ 0\ 0]^T$, $\mathbf{q}_{30} = [0\ \ -20\ 0\ 0\ 0]^T$, $\mathbf{q}_{40} = [0\ \ -40\ 0\ 0\ 0]^T$. Given below is a representation of the transitions.

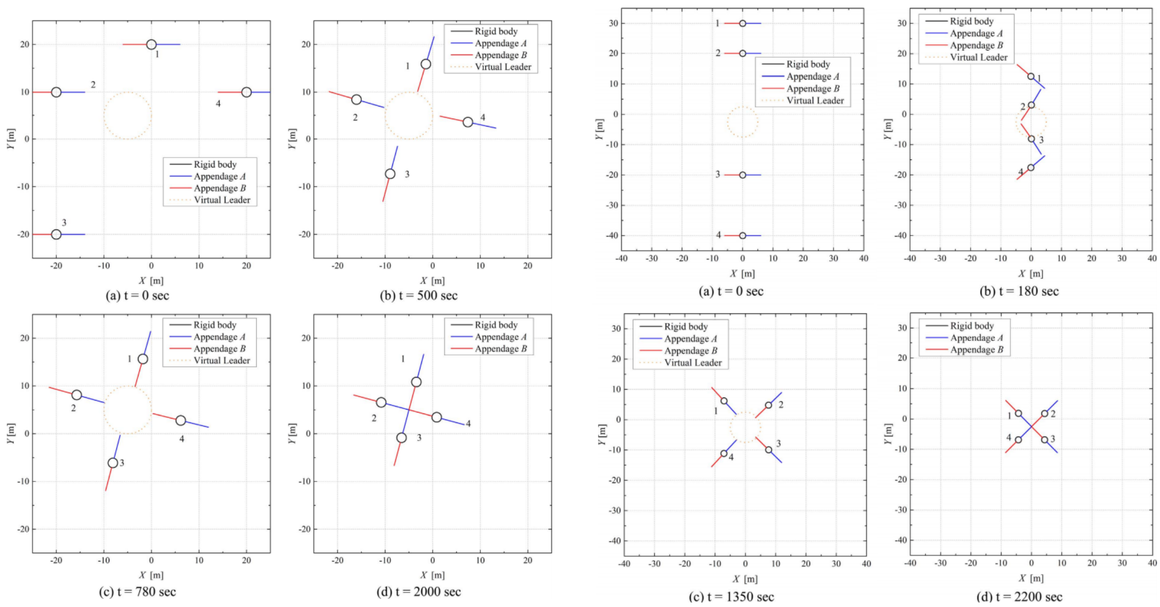

(a) Case 1

(b) Case 2

Figure 6.1: Transitions in the two cases (Chen et al. (2017))

The initial positions are depicted in the $t = 0$ plot for each system. The second graph for each case ($t = 500s$ for (1) and $t = 180s$ for (2)) depicts the time when all the agents are aligned properly but have to translate to the virtual leader, the end of which is depicted by the third graph ($t = 780s$ for (1) and $t = 1350s$ for (2)) when the pre-assembly configuration is achieved. The assembly configuration is achieved at $t = 2000s$ for (1) and $t = 2200s$ for (2) by decreasing the radius of the virtual leader after the pre-assembly configuration is achieved.

Chen and Wen (2018) consider the simulations of two systems. Both systems have six identical flexible spacecrafts with the same parameters for both the agents and the control algorithm, and they differ in the initial positions and orientations of the agents, that for the first system being:

$$\mathbf{x}_{10} = [-100\ -100\ -\pi/2]^T,\ \mathbf{x}_{20} = [-50\ 20\ -\pi/4]^T,\ \mathbf{x}_{30} = [0\ -10\ -\pi/8]^T$$
$$\mathbf{x}_{40} = [30\ 50\ \pi/8]^T,\ \mathbf{x}_{50} = [60\ 0\ \pi/4]^T,\ \mathbf{x}_{60} = [90\ 20\ \pi/2]^T$$

and that for the second system being:

$$\mathbf{x}_{10} = [-100\ -100\ -\pi/2]^T,\ \mathbf{x}_{20} = [-90\ 80\ -\pi/4]^T,\ \mathbf{x}_{30} = [-80\ -60\ -\pi/8]^T$$
$$\mathbf{x}_{40} = [-70\ -40\ \pi/8]^T,\ \mathbf{x}_{50} = [-60\ -20\ \pi/4]^T,\ \mathbf{x}_{60} = [-50\ 0\ \pi/2]^T$$

The Laplacian matrix of the systems according to graph $\mathscr{G}_1$ is given as:

$$L = \begin{bmatrix} 1 & -1 & 0 & 0 & 0 & 0 \\ -1 & 2 & -1 & 0 & 0 & 0 \\ 0 & -1 & 2 & -1 & 0 & 0 \\ 0 & 0 & -1 & 2 & -1 & 0 \\ 0 & 0 & 0 & -1 & 2 & -1 \\ 0 & 0 & 0 & 0 & -1 & 1 \end{bmatrix}$$

The value of the disturbance estimation error converges to zero. Moreover, since the radial Euclidean distances between the spacecrafts are always positive, there is no collision between the agents. In the final step of moving from the pre-assembly configuration to assembly, the hubs only move in the X-direction as expected from the mission planning strategy.

6.3 Spacecraft Attitude Control

Golpashin et al. (2020) consider simulations consisting of a 6U satellite of dimensions $10cm \times 20cm \times 30cm$, maximum mass $6kg$ and entries of the moment of inertia tensor in principal axes $I_1 = 0.05$, $I_2 = 0.065$, and $I3 = 0.025$. The input directions are unit vectors in the three axes. A Monte Carlo experiment is used to compare the results of the proposed stochastic non-linear controller to an LQR controller and to a deterministic non-linear controller ($\varepsilon = 0$). The simulations are performed for 2000 particles on a rest-to-rest maneuver from $x = [0\ 0\ 0\ 1\ 1\ 1]^T$ to $x = [0\ 0\ 0\ 0\ 0\ 0]^T$. Two gain sets are used to study the maneuvers, the first (gain set A) with conservative gains where the strong second condition of the first proposition (pg. 5 in the paper) holds true, and the second (gain set B) with aggressive gains where it need not hold true.

It is noticed that the spectral norm increases with the variance of noise, which is proportional to ε^2. The stochastic controller develops smaller cost than the conventional LQR controller and this generally decreases with increasing order. The decrease in cost for gain set A is not that pronounced when compared to the deterministic controller but again it decreases with increasing order and when compared for gain set B, the decrease is much larger. Gain set B also shows that increasing ε decreases the total cost for the stochastic controller. More aggressive gains and larger spectral norms give higher differences in the total cost, resulting from the 'multiplicative nature of control uncertainty' (a larger thrust gives a higher variation in thrust). The performance of the sextic stochastic controller is plotted against that of the LQR controller measuring the probability of stabilization versus total cost, and it is observed for both gain sets that the former has a higher probability to achieve lower total cost when compared to the latter.

On plotting the trajectories of 100 realizations of the above two controllers for $\varepsilon = 0.2$, we notice that the aggressive gain set B shows a more distinctive improvement in performance for the stochastic controller as well as higher variations such as the case where angular velocity is mostly between ± 0.5 for A but overshoots above 5 for several points in B. The stochastic controller also keeps a smaller difference between the minimum and maximum trajectories, hence setting a stronger constraint on the possible trajectories. Gain set A represents satisfying a strong condition, but there may exist other stable controllers which need not follow the proposition, one of which is represented through B.

The earlier simulations made sure that the initial conditions were within the region of attraction. This is now removed and the initial conditions are set to be within norm 1 of the origin: $x = [0\ 0\ 0\ 0.4\ 0.4\ 0.4]$, $\varepsilon = 0.2$. The system is stable and optimal with a significant decrease in the total cost for the stochastic controller compared to the LQR controller. Here, the strong condition of the proposition is satisfied although the Riccati solution gives entries of magnitude larger than 1. The limitation on initial conditions can be mitigated by having a planning algorithm with reference waypoints at less than norm 1 from each other.

Gui and de Ruiter (2018) have performed simulations on Matlab/Simulink to test the perfor-

mance of the distributed observer. A leader-following spacecraft system is considered with four identical rigid spacecraft as followers and only one follower directly connected to the leader. The leader follows $Q_0(0) = \mathbf{1}$ and $\omega_0(t) = 0.01[sin(\Omega_0 t), cos(\Omega_0 t), sin(\Omega_0 t)]$, where $\Omega_0 = 0.5\ rad/s$. Measurement and communication is quantized in time, and a non-zero disturbance torque is applied on each spacecraft.
The full-state measurements case exhibits fast transient with the leader's trajectory being recovered within 5 seconds. Moreover, it shows some robustness to the small time delays in measurement and communication updates as well as the disturbance torque applied to each spacecraft. Followers reach an agreement with the leader in the attitude-only measurements case as well, and some robustness with respect to disturbances and time delays is again observed. The preprint of the paper presents results with time-varying topologies, and the estimation errors and attitude tracking errors are still convergent indicating the possibility for the distributed observer to be applicable for time-varying topologies as well.

Liu et al. (2020) have performed two simulation, one for testing *coordinated attitude synchronization* and the other for *Coordinated Attitude Tracking*. The former simulation considers four spacecraft, and the network topology randomly switches between four graphs with a retaining time of 10 seconds for each subgraph. The MRPs and angular velocities of each spacecraft are given and θ_i are initialized to zero. Also, the inertia matrix estimate is initialized with a 20% discrepancy. Using the adaptive algorithm gives asymptotically stable attitude synchronization, whereas not using it only bounds the attitudes. The algorithm causes all the angular velocities to converge to zero. Moreover, the control torque and the parameter estimates are bounded.
The second simulation considers a leader in addition to the four spacecraft. Once again, the network topology randomly switching between four graphs with only two having a link between the leader and any other spacecraft. The initial states are also identical, while $\hat{\sigma}_i$ and $\hat{v}_i$ are initialized to zero. The proposed distributed controller and tracking control ultimately achieves coordinate attitude tracking, although the transient is relatively long compared to the synchronization problem (though not much overshoot). Moreover, the control torque and the parameter estimates are bounded as in the previous problem.

Chapter 7

Observations and Conclusions

7.1 Introduction

This chapter presents relevant observations from the research works discussed in the previous chapters. These findings are linked to the problem statement of the project and evaluated based on their applicability. Moreover, the scope of further research is discussed as elaborated in the papers as well as from from personal observations.

7.2 Traditional Concepts on Spacecraft Attitude Control

The textbook on 'Spacecraft Dynamics and Control' deals to a large extent with the concept of attitude control for achieving suitable orbits for the spacecraft. A concept worth noting for the application of formation control is the idea of Euler-Hill equations in Section 2.3.5 wherein satellites close to each other can develop a non-inertial frame of reference that is based on the body frame of any one of the satellites. The equations for $\boldsymbol{\rho} = \boldsymbol{r}_1 - \boldsymbol{r}_2$ can be conjoined with a suitable control law to manage the shape and size of the formation.

Much of the traditional literature on spacecraft attitude control deals with Euler angles, direction cosines, and quaternions, as is observed in Section 2.6.1 of the textbook. A much better approach for attitude control is using the concept of modified Rodrigues parameters as mentioned in Liu et al. (2020). This method uses only three parameters rather than four (as in the case of quaternions), but the singularities that arise from this restriction are at 2π and -2π which can be avoided by switching the parameters as mentioned in Section 5.3.1.

7.3 Basic Concepts on Formation Control

Knorn et al. (2016) present the developments in the field of collective behaviors for multi-agents systems by dealing with the various techniques used in both the time and the network dimensions for such networks. The survey discusses research performed on several aspects of multi-agent control. The topic of formation control is not explained in detail although other useful aspects such as dynamics, topologies and expected non-idealities are discussed.

Oh et al. (2015) delve particularly into the field of formation control. The paper predominantly focuses on displacement-based control using identical agents, and this needs to be studied for heterogeneous agents which is more realistic such as managing the orbits of multiple satellites belonging to different satellite constellations (although position-based control seems easier in this scenario). Issues such as connectivity preservation and collision avoidance need to be handled in both displacement- and distance-based control.
As a result of its communication with a global coordinator using sensing equipment such as GPS receivers, position-based control is expected to be costly. Also, as mentioned in the paper, distance-based control requires the interaction graph to be rigid or persistent. Non-linear systems can complicate stability analysis as well. Though the paper has dealt with distance-based control, a more general study of the field is required in terms of the stability of the rigid (or persistent) system as well as the model used to depict the agent.

Anderson et al. (2007) deal with the specific problem of using a simple cyclic directed graph for formation shape control. The paper shows that persistence of the graph is required for stability and not only rigidity. Separate work by the same authors, Summers et al. (2011) , has dealt with minimally persistent cyclic graphs with more number of agents. However, the control laws are not always stabilizing and different gains need to be given to different agents for stability based on the rigidity matrix.

7.4 Practical Applications of Decentralized Formation

Sakurama et al. (2019) present a solution using distributed control and pattern matching for the problem of formation control using relative positions using local coordinates and bearings, and develops on why clique rigidity is a strict condition to achieve the desired formation. It also considers a gradient-flow approach The paper also provides numerical examples demonstrating the effectiveness of the proposed method and concludes with theorems concerning the sufficiency and the necessity of clique rigidity for achieving the desired formation.

The paper proves that a multi-agent system can converge to a desired formation with clique rigidity even without global rigidity or completeness, as a result of which the graph becomes much simpler. In the case of a spacecraft formation, this is valuable since it will help surpass communication limitations and occlusion of spacecrafts due to the earth.

Ren and Beard (2004) present the problem of decentralized formation control of spacecraft. A virtual structure approach using a bidirectional ring topology is used and the corresponding control laws are developed for controlling both the spacecrafts and the coordination vector instantiations. Simulation results show that using formation feedback gives almost ideal results in spite of actuator saturation.

The concept of the paper is very close to the theme of the project. However, a weakness of this system is that each local instantiation should be synchronized leading to more complexity. Using coordination vectors for information exchange and a ring topology reduces this complexity to some extent. There might also exist discrepancies between the starting time of each instantiation of the agent coordination vector dynamics, and this can be mitigated by using suitable control laws for the coordination vector in each individual agent.

She and Li (2020) present the problem of assembling a large space telescope using multiple manipulators. In order to provide an optimal solution for the path taken by the manipulators, it de-

velops a two-level algorithm and adds in more conditions such as maximizing inter-manipulator distance and introducing time delays for simplifying the process without considering a separate collision detection algorithm. This algorithm has been proven through simulations to perform better than established algorithms on platforms such as MATLAB and C++.
There is only a small hint of formation control in the concept since it deals with robots which construct the telescope rather than self-assembly where formation control would have been essential. Also, the simulations assume that the pieces of the telescope are already placed in the required locations although, in a real-life scenario, the manipulator will have to return to the initial point for collecting the next piece after inserting each piece and this period would have to be included into the algorithm. Apart from these factors, the paper has proposed a proper idea which can possibly be implemented readily into a high-level controller for such a system.

The results obtained by Chen et al. (2017) clearly show that the mechanism can be effective in an ideal environment. However, the paper mentions about shortcomings that may occur due to disturbances, input saturation, etc. due to which a more robust controller needs to be developed for a real-life application. The flexibility of the beams protruding from the rigid hub leads to significant deformation and first-order modal vibrations when the hub starts moving although these vibrations die out as the system reaches stability. Moreover, there seems to be high vibrations in the control variables T_o acting on the rigid hubs which subsequently reduce.

Having been written by the same authors and with similar objectives, the problem of the paper by Chen and Wen (2018) and several concepts from the methodology are very similar to the previous paper. The proposed compound controller consists of an assembly controller that follows a fixed graph (which is based on the numbering of the agents) and a collision avoidance controller that follows a time-variant graph (which is modified based on the distance between the agents). The assembly controller considers the effect of disturbance due to the non-observed vibrations of the two appendages that stick out from the rigid hub. As a result, it utilizes a disturbance observer which approximates to the actual disturbance as proven using the Lyapunov stability theorem and as displayed on the case studies.
The proposed controller is simple and easy to implement as is visible from the fact that modifying the parameter Δ can allow the multi-agent system to achieve any collision-free final

configuration in two-dimensional space. Moreover, it can be scaled to a huge multi-agent network. However, it does not consider practical difficulties such as three-dimensional assembly, realization of sensors and actuators, and computational complexity.

7.5 Recent Developments in Spacecraft Attitude Control

Golpashin et al. (2020) present a stochastic non-linear controller which performs better than an LQR controller and a deterministic non-linear controller in several aspects. It is shown that the total cost reduction is improved with increasing non-linearity of the controller and increasing noise variance. The paper suggests how such a controller with desirable disturbance suppression properties can be used in space applications such as docking where torque disturbances could be unwanted or even hazardous.

Gui and de Ruiter (2018) propose a non-linear distributed observer that recovers the leader's trajectory (attitude and angular velocity) in finite time for each follower provided a fixed topology and no time delays. This observer is integrated with single-spacecraft controllers with full-state measurements and attitude-only measurements for global group attitude agreement. The observer is simulated to test convergence of the errors, and positive results are obtained in both cases even with disturbances and time delays.

Liu et al. (2020) develop algorithms for coordinated attitude synchronization and coordinated attitude tracking, where agents are unaware of their inertial parameters and the network topology graph switches although satisfying uniform joint connectivity for attitude synchronization and uniform joint quasi-strong connectivity for tracking. An adaptive controller is developed for the former problem such that the inertial parameter is estimated along with the control torque. The tracking problem is solved in two steps: distributed observer design to estimate the MRPs and velocity of the leader, and tracking control development for attitude tracking.
The techniques presented in the paper help reduce the load on interaction capabilities by actively cutting the interaction connection regularly. This is useful since power concerns may preclude a strong interaction between every spacecraft. The system is also made robust against abrupt link disconnection from environmental factors, which is very probable for spacecraft formations.

Chapter 8

Future Scope and Personal Learnings

8.1 Introduction

The field of multi-agent formation control has been predominantly dealt using simple models such as single- and double- integrators as observed throughout the paper by Oh et al. (2015). Research independent of this field has also introduced the concept of attitude control in great detail. Concepts learned from the literature survey done in this project can be used to develop decentralized formation control of spacecraft using optimal attitude control strategies. This chapter deals with techniques and strategies that can be adopted in this direction.

8.2 Future Prospects

As observed in Section 2.3.5 and referenced in 7.2, the concept of Euler-Hill equations can be utilized in controlling the distance of heading of spacecraft in a formation.
A large fraction of research papers discussed in this thesis explain why and/or how the proposed concept can be improved. Knorn et al. (2016) discuss several prospects of research in collective

behaviors such as:

- Developing the requirements on synchronization for nonlinear and heterogeneous agents in complicated networks without being governed by a 'homogeneous kernel';
- considering direct physical coupling that usually exists among agents, hence disregarding the assumption that all agents are autonomous; and
- developing the behavior of multi-agent systems in both the time and the network dimensions for two-dimensional collective behaviors.

The concept that Anderson et al. (2007) develops on the control of a co-leader system is a direct application of distance-based control. This can be developed to a three-dimensional setting to achieve realistic decentralized control.

In their work on multi-agent coordination via distributed pattern matching, Sakurama et al. (2019) discuss how the concept of relative states can be generalized to extend the class of observable outputs, such that they match the requirements from controller design in practical applications. On the application-based perspective, Ren and Beard (2004) mentions how the issue of time delay in information exchange between neighboring spacecrafts has not been dealt with and is kept open for further research in the problem of decentralized formation flying using a virtual structure approach. Also, in the paper on on-orbit spacecraft assembly using potential field, although Chen et al. (2017) mention the disjunction between the problem and general spacecraft formation control, a similar artificial potential field may be developed for distance-based control. Similar to the formation control problem, the problem statement in the paper constrains the motion of agents into a given state using a simple and feasible mechanism.

The work on attitude synchronization and tracking control with switching communication network topologies by Liu et al. (2020) has to be extended with the inclusion of communication problems such as delay, packet loss and distortion. From the research work by Golpashin et al. (2020) on thrust uncertainty in attitude control, it may be a good idea to use the optimal control algorithm in developing a controller for individual spacecrafts in a multi-spacecraft formation. Moreover, the observer presented in the paper by Gui and de Ruiter (2018) is very useful for a real-life formation control problem involving spacecraft since not all followers will be able to directly connect to the leader. However, this system has not been proven to function for all time-varying topologies or time-delayed links though these can be expected since the spacecrafts work on clocked controllers and may be at very large distances from each other.

8.3 Personal Learnings from the Project

This project has personally been a novel experience in several manners. First of all, it introduced me to a very practical problem that captured my imagination. The applications of decentralized control are widespread, from small Kobuki robots to enormous satellites and spaceships. And decentralized formations with attitude control is especially applicable for managing spacecraft and satellites in earth orbits. Very soon, with technological developments and commercial voyages, outer space will be as crowded as today's airspace. A control scheme that helps achieve the desired goal without collisions will be a necessity, and I believe that this work will have a significant role in that application.

Secondly, the project helped me look around into nature and made me realize how decentralized multi-agent control has always been there around us, from social insects like ants and honey bees to complex formations such as murmurations. It is fascinating to observe how the cooperative control of multiple agents can be more effective than individual labor, and I believe that, in the future, such systems can have much wider roles in our lives.

Throughout the entire course of the project and thesis preparation, I was fortunate to follow the basic tenet of research: standing on the shoulders of giants and developing thereafter into domains unknown. It is a common mistake to perform research without a prior understanding of the work that has already been done in the field. Thanks to my advisor, I was able to get a lay of the land instead of prematurely attempting to deal with complex problems.

Finally, the mathematical rigor that each research work posed was indeed a challenge at some instances, but they have helped me understand concepts that are actively used for solving research problems, concepts that are not usually taught through textbooks in lectures but are required to be self-learned. As mentioned previously, I would never have realized the depth of this field if not for the literature survey involved in the project.

In general, the project has been an amazing experience and has made an enormous impact on my academic life.

Appendix A

Glossary

Barbalat's Lemma : Suppose $f(t) \in C^1(a,\infty)$ and $\lim_{t\to\infty} f(t) = \alpha$ where $\alpha < \infty$. The lemma states that, if f' is uniformly continuous, then $lim_{t\to\infty} f'(t) = 0$. [1]

Cactus graph : A cactus graph is a pair of distinct simple circuits have at most one common vertex.[2]

Containment control problem : The containment control problem involves driving followers into the convex hull spanned by dynamic leaders.[2]

Cut-balanced topology : A cut balanced topology is one where the influence of remaining groups on a group of agents is proportional to its influence on the remaining ones.[2]

Euler-Bernoulli beam assumptions : The Euler-Bernoulli beam assumptions are: [3]

- Cross sections of the beam do not deform in a significant manner under the application of transverse or axial loads and can be assumed as rigid

[1] ASU | Hao Liu | Things You Probably Would Not Want To Explain To Your Parents | Barbalat's Lemma
[2] Oh et al. (2015)
[3] MIT 16.20 | Module 7 - Simple Beam Theory

- During deformation, the cross section of the beam is assumed to remain planar and normal to the deformed axis of the beam.

H2 norm : The H2 norm of a stable system H is the root-mean-square of the impulse response of the system.[4]

Genetic Algorithm : The genetic algorithm is a method for solving both constrained and unconstrained optimization problems based on natural selection; i.e., by repeatedly modifying a population of individual solutions. At each step, individuals are selected at random from the current population to be parents and are used to produce the children for the next generation. Over successive generations, the population "evolves" toward an optimal solution.[5]

Hausdorff distance : The Hausdorff distance between two sets of numbers $A = \{a_1, a_2, ..., a_n\}$ and $B = \{b_1, b_2, ..., b_m\}$ is the smallest value d such that every point of A has a point of B within distance d and every point o f B has a point of A within distance d, where [6]

$$d(A,B) = max\{\max a \in A \min b \in B|b-a|, \max b \in B \min a \in A|a-b|\}$$

Lipschitz condition : Function $f(t,y)$ satisfies a Lipschitz condition in the variable y on a set $D \subset \mathbb{R}^2$ if a constant $L > 0$ exists with $|f(t,y_1) - f(t,y_2)| \leq L|y_1 - y_2|$, whenever (t,y_1), (t,y_2) are in D. Here, L is Lipschitz constant.[7]

Modified Rodrigues parameters (MRPs) : $\sigma_i = \eta_i \tan(\frac{\phi_i}{4}) \in \mathbb{R}^3$ for the i-th spacecraft, where $\eta \in \mathbb{S}^2$, $\phi_i \in (-2\pi, 2\pi)$ are the corresponding Euler axis and angle resp.

Network integrity : Network integrity is defined as the ability of the network to support a desired communication rate.[2]

Relative and Distributed gradients : A continuous function $v(X)$ is said to have a relative gradient if it is differentiable almost everywhere and for $i \in \mathscr{V}$, there exists a function $\bar{f}_i$ such that

[4]MathWorks Help Center | Resources | norm

[5]MathWorks Help Center | Documentation | What Is the Genetic Algorithm?

[6]Rote (1991)

[7]UC Berkeley | MA128A Spring 2017 Notes | Week 9

$\frac{\partial v}{\partial x_i}(X) = -R_i \bar{f}_i([R_i^T(x_j - x_i)]_{j \in V \setminus \{i\}})$. $\mathscr{F}_r$ is the set of all continuous functions having relative gradients. A continuous function $v(X)$ is said to have a distributed gradient if it is differentiable almost everywhere and for $i \in \mathscr{V}$, there exists a function $\tilde{f}_i$ such that $\frac{\partial v}{\partial x_i}(X) = -\tilde{f}_i(x_i, [x_j]_{j \in \mathscr{N}_i})$. $\mathscr{F}_d(G)$ is the set of all continuous functions having distributed gradients over G. [8]

Standard (1-D) Wiener process (or Brownian motion) : Brownian motion involves a stochastic process $\{W_t\}_{t \geq 0+}$ indexed by non-negative real numbers t such that:

- $W_0 = 0$,
- with probability 1, the function $t \to W_t$ is continuous in t,
- the process $\{W_t\}_{t \geq 0}$ has stationary, independent increments, and
- the increment $W_{t+s} - W_s$ follows the $normal(0,t)$ distribution [9]

Stochastic Differential Equations : The problem of solving stochastic differential equations involves solving the differential equation of the form: [10]

$$dX = \mu(t, X(t))dt + \sigma(t, X(t))dB(t)$$

for given functions a and b, and a Brownian motion $B(t)$. A function (or a path) X is a solution to the differential equation above if it satisfies:

$$X(T) = \int_0^T \mu(t, X(t))dt + \int_0^T \sigma(t, X(t))dB(t)$$

Switching Graph : A switching graph $\mathscr{G}_{\zeta(t)} = \{\mathscr{V}, \mathscr{E}_{\zeta(t)}\}$ consists of a node set $\mathscr{V} = \{1, 2, ..., n\}$ and a time varying edge set $\mathscr{E}_{\zeta(t)} \subseteq \mathscr{V} \times \mathscr{V}$, where $\zeta(t)\colon [0, \infty) \to \mathscr{H}$ is piecewise constant and set $\mathscr{H} = \{1, 2, ..., \hbar\}$ includes all possible graphs ($\hbar$ is some positive integer), s.t. the graph switches at discrete time instances.

[8]Sakurama et al. (2019)

[9]UChicago | Statistics 313 (Stochastic Processes II) | Lecture Notes G

[10]MIT 18.S096 | Lecture 21 - Stochastic Differential Equations

Tsiotras-Longuski Parameterization for orientation : The rotation matrix from the inertial frame to the body frame is given as $R = R_1(z)R_2(w)$ with

$$R_1(z) = \begin{bmatrix} cos(z) & sin(z) & 0 \\ -sin(z) & cos(z) & 0 \\ 0 & 0 & 1 \end{bmatrix}$$

$$R_2(w) = \frac{1}{1+w_1^2+w_2^2} \begin{bmatrix} 1+w_1^2-w_2^2 & 2w_1w_2 & -2w_2 \\ 2w_1w_2 & 1-w_1^2+w_2^2 & 2w_1 \\ 2w_2 & -2w_1 & 1-w_1^2-w_2^2 \end{bmatrix}$$

where $z \in \mathbb{R}$ is a rotation about the body z-axis, and $w = w_1 + iw_2 \in \mathbb{C}$ gives the coordinates for a point on the complex plane. The stereographic projection of the rotated z-axis onto the complex plane gives $w = \frac{b-ia}{1+c}$ where (a,b,c) are the direction cosines of the rotation. Since $R_1(z), R_2(w) \in SO(3)$, the parameterization gives a singularity at $w_1, w_2 \to \infty$. The evolution of w and z is given by the following differential equations: [11]

$$\begin{bmatrix} \dot{w}_1 \\ \dot{w}_2 \\ \dot{z} \end{bmatrix} = \begin{bmatrix} \frac{1}{2} & 0 & w_2 \\ 0 & \frac{1}{2} & -w_1 \\ -w_2 & w_1 & 1 \end{bmatrix} \begin{bmatrix} \omega_1 \\ \omega_2 \\ \omega_3 \end{bmatrix} + \begin{bmatrix} \frac{1}{2}(w_1^2-w_2^2) & w_1w_2 & 0 \\ w_1w_2 & \frac{1}{2}(-w_1^2+w_2^2) & 0 \\ 0 & 0 & 0 \end{bmatrix} \begin{bmatrix} \omega_1 \\ \omega_2 \\ \omega_3 \end{bmatrix}$$

[11]Golpashin et al. (2020)

References

Anderson, B. D., Yu, C., Dasgupta, S., Stephen Morse, A., 2007. Control of a three-coleader formation in the plane. Systems Control Letters 56 (9), 573 – 578.

Beard, R. W., Lawton, J., Hadaegh, F. Y., 2001. A coordination architecture for spacecraft formation control. IEEE Transactions on Control Systems Technology 9 (6), 777–790.

Chen, T., Wen, H., 2018. Autonomous assembly with collision avoidance of a fleet of flexible spacecraft based on disturbance observer. Acta Astronautica 147, 86 – 96.

Chen, T., Wen, H., Hu, H., Jin, D., 2017. On-orbit assembly of a team of flexible spacecraft using potential field based method. Acta Astronautica 133, 221 – 232.

Golpashin, A. E., Yeong, H. C., Ho, K., Sri Namachchivaya, N., 2020. Spacecraft attitude control: A consideration of thrust uncertainty. Journal of Guidance, Control, and Dynamics 43 (12), 2349–2365.

Gui, H., de Ruiter, A. H., 2018. Global finite-time attitude consensus of leader-following spacecraft systems based on distributed observers. Automatica 91, 225 – 232.

Knorn, S., Chen, Z., Middleton, R. H., 2016. Overview: Collective control of multiagent systems. IEEE Transactions on Control of Network Systems 3 (4), 334–347.

Liu, X., Zou, Y., Meng, Z., You, Z., 2020. Coordinated attitude synchronization and tracking control of multiple spacecraft over a communication network with a switching topology. IEEE Transactions on Aerospace and Electronic Systems 56 (2), 1148–1162.

Oh, K.-K., Park, M.-C., Ahn, H.-S., 2015. A survey of multi-agent formation control. Automatica 53, 424 – 440.

Ren, W., Beard, R. W., 2004. Decentralized scheme for spacecraft formation flying via the virtual structure approach. Journal of Guidance, Control, and Dynamics 27 (1), 73–82.

Rote, G., 1991. Computing the minimum hausdorff distance between two point sets on a line under translation. Information Processing Letters 38 (3), 123 – 127.

Sakurama, K., Azuma, S., Sugie, T., 2019. Multiagent coordination via distributed pattern matching. IEEE Transactions on Automatic Control 64, 3210–3225.

She, Y., Li, S., 01 2020. In-orbit robotic assembly mission design and planning to construct a large space telescope.

Sidi, M. J., 1997. Spacecraft Dynamics and Control: A Practical Engineering Approach. Cambridge Aerospace Series. Cambridge University Press.

Summers, T. H., Yu, C., Dasgupta, S., Anderson, B. D. O., 2011. Control of minimally persistent leader-remote-follower and coleader formations in the plane. IEEE Transactions on Automatic Control 56 (12), 2778–2792.

Young, B. J., Beard, R. W., Kelsey, J. M., 2001. A control scheme for improving multi-vehicle formation maneuvers 2, 704–709 vol.2.